

1 **Forearc crustal faults using and estimated worst-case**  
2 **tsunami scenario-sources in the upper plate of the**  
3 **Lesser Antilles subduction zones. The Case study of the**  
4 **Morne Piton fFault system. ~~(Lesser Antilles,~~**  
5 **~~Guadeloupe Archipelago).~~**

6 Melody Philippon<sup>1,\*</sup>, Jean Roger<sup>2</sup>, Jean-Frederic. Lebrun<sup>1</sup>, Isabelle Thinon<sup>3</sup>, Océane Foix<sup>4</sup>,  
7 Stéphane Mazzotti<sup>4</sup>, Marc-Anadre Gutscher<sup>5</sup>, Leny Montheil<sup>4</sup>, Jean-Jacques Cornée<sup>4</sup>.

8 *1. Géosciences Montpellier, Université de Montpellier, CNRS, Université des Antilles, Pointe-*  
9 *à-Pitre, French West Indies.*

10 *2. Earth and Structure Processes Department, GNS Sciences, Lower Hutt, New Zealand.*

11 *3. BRGM – French Geological survey, 3 avenue Claude Guillemin 45060 Orléans*

12 *4. Géosciences Montpellier, Université de Montpellier, CNRS, Université des Antilles,*  
13 *Montpellier, France.*

14 *5. Geo-Ocean, Univ.Brest, CNRS, Ifremer, Brest, France.*

15 *\* Corresponding author : melody.philippon@univ-antilles.fr*

16  
17 ***Abstract***

18 In this study, alternatively to the megathrust, we identify upper plate normal faults  
19 orthogonal to the trench as a possible tsunami source along the Lesser Antilles  
20 subduction zone. ~~We study t~~The Morne Piton fFault system, is such a trench-  
21 perpendicular upper crustal fault ~~affecting the Lesser Antilles forearc~~ at the latitude of  
22 Guadeloupe. By the means of seismic reflection, high resolution bathymetry, ~~R~~remotely  
23 ~~O~~perated ~~V~~ehicle (ROV) ~~images~~ and dating, we reassess the slip rate of the Morne  
24 Piton fFault ~~since 7Ma, i.e. its inception, 7My ago and quantify an average rate of at~~ 0.25  
25 mm.yr<sup>-1</sup>mm.yr<sup>-1</sup> since ~~ca. 1.2Ma fault inception (i.e. 7 Ma),~~ dividing by two five previous  
26 estimations and thus increasing the earthquake time recurrence and lowering the  
27 associated hazard. ~~We evidence~~ROV dives revealed a metric scarp with striae at the toe  
28 of the Morne Piton fFault system suggesting a recent fault rupture. We estimate a fault  
29 rupture area of ~ 450-675 km<sup>2</sup> and then a magnitude range for ~~the a maximum~~ seismic  
30 event around M<sub>w</sub> 6.5 ± 0.5 making this fault potentially tsunamogenic as the nearby Les

31 ~~Saintes Fault responsible for a tsunami following the 2004,  $M_w$  6.43 earthquake.~~  
32 ~~Consequently we simulate~~ We present results from a multi-segment tsunami model  
33 representative for ~~the a~~ worst-case scenario ~~which gives an overview of what could~~  
34 ~~happen in terms of tsunami generation as~~ if the whole identified Morne Piton fFault  
35 segments ruptured together. Our model ~~illustrates~~ provides clues for the potential impact  
36 of local tsunamis on the surrounding coastal area as well as for local bathymetric controls  
37 on tsunami propagation. We illustrate that as (i) shallow water plateaus act as secondary  
38 sources and are responsible for a wrapping of the tsunami waves around the island of  
39 Marie-Galante, (ii) canyons indenting the shallow water plateau slope break are focusing  
40 and enhancing the wave height in front of the most touristic and populated town of the  
41 island, (iii) a resonance phenomenon is observed within Les Saintes archipelago showing  
42 that the waves' frequency content is able to perturbate the sea-level during many hours  
43 after the seismic rupture.

44  
45 Keywords: subduction zone, forearc, crustal fault, slip rate, tsunami hazard, Lesser  
46 Antilles, Guadeloupe Island

## 48 **1. Introduction**

49  
50 Regions at the vicinity of active subduction zones are prone to seismic and related  
51 hazards, including tsunamis, exposing their inhabitants to multiple threats. Megathrust  
52 earthquakes represent the greatest threat with the highest seismic moments and  
53 consequently huge tsunamigenic potential (Satake and Tanioka, 1999). Earthquakes  
54 triggered on crustal faults in the overriding plate represent an additional hazard that  
55 needs to be quantified (Bilek, 2010). In order to assess the hazards and mitigate the risks  
56 associated with these crustal faults, it is essential to estimate their slip rates.

57 On land, slip rates on active faults are determined from paleo-seismic trenches (McCalpin,  
58 1996), high resolution geophysical investigation (Wallace, 1981; Zhang et al., 2014),  
59 satellite imagery (Tronin, 2009), InSAR (Biggs and Wright, 2020), geodetic measurement  
60 (GNSS: Symithe et al., 2013) as well as seismicity which account for the present-day strain  
61 accumulation of the crust. Offshore, slip rate estimates are provided by the means of  
62 underwater geodesy (*i.e.* acoustic geodesy: Kido et al., 2006; Petersen et al., 2019; Fujita  
63 et al., 2006) or fiber optic monitoring (Hirata et al., 2002; Gutscher et al., 2019). **Event**

64 ~~time~~The recurrence time of events may be estimated by the study of turbidite deposits  
65 cores (e.g., Cascades: Goldfinger et al., 2012; Taiwan: Lehu et al., 2016; Antilles: Seibert et  
66 al., 2016; New Zealand: Lewis et al., 1980), high resolution marine seismic and multibeam  
67 echo-sounder data (e.g., Escartin et al., 2016, 2018), and submarine dives survey (e.g.,  
68 Geli et al., 2011). However, constraining hazard models in areas undergoing slow strain  
69 rates remains challenging as the earthquakes recurrence time overcomes the historical  
70 period. Indeed, geodetic measurements require decades-long time series as the  
71 resolution of the method is not accurate enough and erosion or high sedimentation rates  
72 may have erased or covered, respectively, the active fault scarps making it difficult to  
73 identify active faults segments. Therefore, datasets based on the last ten to hundred years  
74 of record along tectonic systems undergoing slow strain rates may not be representative  
75 of the bulk strain and may be at the origin of biased estimations of slip rate along these  
76 faults.

77 The Lesser Antilles (Eastern Caribbean) records slow deformation rates as the north and  
78 south American tectonic plates slowly subduct under the Caribbean plate (20mm·yr<sup>-1</sup> -  
79 Figure 1). Extensional tectonics and normal faulting affect the forearc (Feuillet et al.,  
80 2002, De Min et al., 2015, Boucard et al., 2021) but available historical data do not report  
81 tsunami events related to forearc fault rupture. However, the Les Saintes M<sub>w</sub> 6.3  
82 earthquake of December 2004 ruptured the Roseau normal fault (Feuillet et al., 2011a,  
83 Bazin et al., 2010). The earthquake reached an intensity up to VIII in the Guadeloupe  
84 Archipelago (Figure 1), being felt by most of its ~400,000 inhabitants, and was  
85 responsible for one casualty. This earthquake triggered a tsunami with up to 2\_m high  
86 waves at the coast and a maximum measured run-up distance of 42 m in Les Saintes  
87 (Zahibo et al. 2005; Le Friant et al. 2008; Cordrie et al. 2020). Prior to this event, this fault  
88 was unmapped and therefore not identified as an active fault (Feuillet et al., 2002; Terrier  
89 and Combes, 2002). Forearc normal faults, similar to Les Saintes fault system, may pose  
90 a threat to the 4 million inhabitants of the Lesser Antilles that are living on 17-volcanic  
91 arc islands facing the subduction trench to the east and literally sitting over the  
92 subduction interface.

93 The present study focuses on the Morne Piton fFault system, perpendicular to the  
94 subduction trench, which is one of the most prominent onshore-offshore fault systems  
95 which cuts the Guadeloupe Archipelago arc and forearc islands (Figure 1). Regarding the  
96 seismic and tsunami hazards related to this fault system and the vulnerability of the

97 coastal population and infrastructures of the archipelago, the objectives are to (1)  
98 estimate the fault slip rate (2) determine the geometry of the fault segments, and (3)  
99 model the associated tsunami hazard, since such a joint approach has been lacking so far.  
100 In the following study, the fault geometry is refined in order to provide an up-to-date map  
101 of the fault segments thanks to high-resolution (HR) bathymetric data. Then, we integrate  
102 its long-term slip rate over the last *ca.* 7 My, *i.e.* from fault initiation to present-day, by the  
103 mean of HR seismic reflection lines and available ~~or recent~~ biostratigraphic and isotopic  
104 dates. Secondly, Remotely Operated Vehicles (ROV) explorations of seafloor rupture  
105 allowed us to measure the height of the fault scarp and to determine the fault kinematics  
106 from striations ~~observed along a corresponding to the most recent earthquakesco-~~  
107 ~~seismic scarp. Because T~~the overall geometry of this fault system is comparable to the Les  
108 Saintes fault system in terms of length, seafloor scarp and dip. ~~We thus~~ postulate that  
109 a rupture along the Morne Piton ~~f~~Fault may trigger a local tsunami, close to the coasts of  
110 the Guadeloupe Archipelago. ~~Therefore Then,~~ we ~~assess discuss study~~ the seismogenic  
111 and tsunamigenic potential of the Morne Piton ~~f~~Fault system providing an overview of  
112 what could happen in terms of tsunami generation if all the segments of the Morne Piton  
113 ~~f~~Fault ruptured simultaneously, *i.e.* a plausible worst-case scenario. ~~We further~~~~This~~  
114 ~~scenario permitallows to identify and~~ -discuss the local bathymetric controls on the  
115 propagation of the ~~ensuing resulting~~ tsunami wave and the consequences (*e.g.*,  
116 amplifications and interferences) in near-shore areas of the neighboring ~~highly~~ populated  
117 islands. ~~We do not assess coastal inundation scenarios, as our scenario can't be refined~~  
118 ~~by observational rupture data accurate enough to realize such a riskspecific hazard study.~~  
119 Finally, we ~~reassess conclude on~~ the importance of forearc crustal faults as potential  
120 major tsunami sources in subduction zones ~~worldwide~~.

121

## 122 **2. Geological settings**

123

124 Oceanic lithosphere of the North and South American plates is slowly subducting  
125 beneath the Caribbean plate at a convergence rate of  $\sim 20 \text{ mm} \cdot \text{yr}^{-1}$  (Figure 1, DeMets et  
126 al., 2000; ~~Feuillet et al., 2001~~; Philippon and Corti, 2016). The convex trench geometry  
127 results in along strike variations of obliquity, increasing northward from Guadeloupe.  
128 Along the arc, ~~at the latitude of Guadeloupe~~, oblique subduction is accommodated by  
129 trench-parallel left-lateral strike slip faults such as the ~~Harvers-~~Montserrat-Bouillante /

130 Les Saintes corridor (located within the volcanic arc), the Bunce fault (located along the  
131 crustal buttress), and a series of trench-perpendicular grabens forming a sinistral  
132 horsetail (Feuillet et al., 2002; Feuillet et al., 2010; Ten Brink et al., 2004; Laurencin et al.,  
133 2019; Boucard et al., 2021) (Figure 1, Figure 2A).

134 In the central Lesser Antilles, the Marie-Galante Basin (Guadeloupe Archipelago),  
135 is located at the southern end of the aforementioned regional horsetail system and is  
136 described as a conjugated normal fault system defining a trench perpendicular graben  
137 (Figure 2 A; Feuillet et al., 2001, 2011). This graben affects sediment deposits comprising  
138 three regional mega-sequences: an Eocene(?) - Early Miocene MG-MS1 sequence, a mid-  
139 Miocene – late Tortonian / early Messinian MG-MS2 sequence, and a Messinian to present  
140 MG-MS3 sequence (Bouysse et Mascle, 1994; De Min, 2014; De Min et al., 2015; Cornée et  
141 al., 2023). It shapes the Marie-Galante Basin (up to 1200 m water depth) and  
142 surroundings, Grande-Terre and Marie-Galante Islands, respectively (Figure 1). The  
143 northern boundary of the Marie-Galante Basin is the east trending, south dipping Gosier  
144 fault that runs primarily onshore along the southern coast of Grande-Terre (Garrabé and  
145 Andreieff, 1988; and Figure 2A). The southern boundary of the basin consists of the  
146 N100° trending, ~50 km-long, north dipping Morne Piton fFault, which crosscuts the  
147 northern edge of Marie-Galante Island (Bouysse et al., 1993) and extends offshore on both  
148 sides of the island (Feuillet et al., 2002, 2004).

149 The Morne Piton fFault system consists of five main 5-15 km-long segments  
150 trending N90°E ± 30° separated by N140°E shorter right-lateral relays (Figure 2). The  
151 fault scarp is exposed at Anse Piton, eastern coast of Marie-Galante, and shows dip-slip  
152 striations (Feuillet et al., 2002). Onshore Marie-Galante, the fault offsets the Pliocene to  
153 middle Pleistocene platform by ~60 m. It also crosscuts a series of 3 uplifted late-mid to  
154 late Pleistocene terraces along the eastern side of the island. Feuillet et al. (2004)  
155 calculated a 5 km dislocation depth and a 70 to 80°N fault dip to model the observed  
156 flexure of the footwall. Considering that the Marie-Galante Plateau is a flat abandoned  
157 330 Ka old marine terrace, these authors estimate the average slip rate of the Morne Piton  
158 at about  $0.5 \pm 0.2 \text{ mm}\cdot\text{yr}^{-1}$  since 330 Ka. Regarding the uplifted terraces they  
159 estimated a maximum earthquake moment magnitude ( $M_w$ ) ranging from 5.8 up to 6.5  
160 with a 400-1000 to 1400-3300 years of recurrence time, respectively (250 km<sup>2</sup> of  
161 estimated ruptured area). Moreover, it was later demonstrated that this plateau emerged  
162 between 1.77 and 1.07 Ma (magnetostratigraphic Chron 1R2r; Cornée et al., 2012; Münch

163 et al., 2014; De Min et al., 2015; Léticée et al., 2019; Cornée et al., 2021). Note that  
164 considering an older age for the Plateau emergence would drastically lower the slip rate  
165 estimate and increase the recurrence time calculated by Feuillet et al. (2001).

166

### 167 ***3. Historical seismicity***

168

169 Upper plate seismicity in the Marie-Galante Basin provided by (i) CDSA Seismic  
170 database (Antilles Seismological Data Center - Bengoubou-Valerius et al. (2008); Massin et  
171 al.(2021)), (ii) IRIS database (IRIS <https://www.isc.ac.uk> (Figure 2B) and (iii) the  
172 deployment of Ocean Bottom Seismometers (OBS) (Ruiz et al., 2013; Bie et al., 2019)  
173 shows a widely distributed pattern of moderate magnitude earthquakes ( $M_w \leq 5.3$ ), with  
174 the exception of the 2004 seismic cluster in Les Saintes. Wide Angle Seismic (WAS)  
175 profiles together with earthquakes data indicate a seismogenic crustal thickness limited  
176 to the first 15-20 km west of Marie-Galante suggesting a brittle-ductile transition at this  
177 depth (Kopp et al., 2011; Ruiz et al., 2013; Gonzalez et al., 2017; Padron et al., 2021).  
178 Among the very few focal mechanisms available in the Marie-Galante Basin (Gonzalez et  
179 al., 2017), the 25 February 2014  $M_w$  3.8 earthquake occurred beneath the southern  
180 Grande-Terre platform and shows pure normal motion along sub-E-W trending nodal  
181 planes (Gonzalez et al. 2017, Event n°9, hypocentral location accuracy of ca. 5 km; Figure  
182 2C). The location, depth and nodal plane characteristics ( $57^\circ$  dip and  $N102^\circ E$ ) of the  
183 earthquake indicate that the event may correspond to a rupture along the Gosier fault  
184 system, which is the only major fault system in the vicinity of the hypocentral location  
185 able to trigger such magnitude earthquake. Feuillet (2000) provided more than 20 focal  
186 mechanisms for earthquakes showing local magnitude  $2 < M_l < 3.7$  and one  $M_s = 5.6$   
187 earthquake, located in and around the Marie-Galante Graben. All focal mechanisms show  
188 nearly pure normal motion along sub-E-W trending nodal planes, consistent with  
189 kinematics indicators observed along the Gosier and Morne Piton faults. This tectonic  
190 pattern is confirmed by GNSS velocities which indicate that a small trench-parallel  
191 extension is accommodated in the upper plate forearc (van Rijsingen et al., 2021).

192 Two historical earthquakes are reported along these two fault systems (Feuillet et  
193 al., 2011b): (i) the 16 May 1851 earthquake with a maximum intensity of VII recorded in  
194 the southeastern part of Basse-Terre, is attributed to the Morne Piton fault with an  
195 estimated moment magnitude  $M_w = 6.0$  (Feuillet et al., 2011b); and (ii) the 29 April 1897

196 earthquake with a maximum intensity of VIII recorded in the Pointe-à-Pitre area being  
197 either attributed to the Gosier Fault system with an estimated moment magnitude  
198  $M_w$  ~~$M_w$~~ =5.5, or to the Montserrat fault zone, with an estimated moment magnitude  
199  $M_w$  ~~$M_w$~~ =6.5 (Bernard and Lambert, 1988; Feuillet et al., 2011b). Overall, at the latitude of  
200 Guadeloupe, regional earthquake data suggests that normal fault systems are active with  
201 an ability ~~of to generating generate earthquakes of moment magnitude  $M_w$  $M_w$  6 and~~  
202 ~~above earthquakes potentially able to trigger tsunami~~This magnitude range is potentially  
203 able to trigger tsunami according to tsunami catalogues -(as explained, for example, in  
204 Roger et al., 2019).

205  
206

#### 207 **4. Historical tsunami**

208

209 Southwest of the Marie-Galante Basin, the 2004  $M_w$  ~~$M_w$~~ 6.3 earthquake (Bazin et  
210 al., 2010; Feuillet et al., 2011) showed that upper plate crustal faults can generate strong  
211 earthquakes and tsunamis. The main shock occurred along the NNW-SSE trending, *ca.* 40  
212 km-long arc-parallel Les Saintes Fault System (Feuillet et al., 2011; Leclerc et al., 2016).  
213 The recurrence of such a rupture is estimated to be a few hundred years or more (Escartin  
214 et al., 2016; Escartin et al., 2018; Feuillet et al., 2011; Le Friant et al., 2008). Focal  
215 mechanisms of the main shock as well as five aftershocks provided an overall pure  
216 normal motion along NNW-SSE nodal planes (Figure 2D). Source models from Salichon  
217 et al. (2009), Bazin et al. (2010), and Feuillet et al. (2011), well constrained by the long  
218 duration of the aftershock sequence, proposed a main source localized along the N135°E  
219 trending, 50°E dipping Roseau Fault (westernmost fault of Les Saintes fault system) with  
220 a 30 km-long and 21 km-down dip width fault plane. Aftershock seismicity reactivated  
221 several nearby conjugate faults with a maximum seismic depth at *ca.* 15 km. The main  
222 rupture occurred at two asperities located 8 km below the surface with a maximum slip  
223 of 1.8 m, and propagated to the surface triggering a coseismic offset of the seafloor of 0.3-  
224 0.6 m along a *ca.* 10 km-long segment. Escartin et al. (2016) investigated the fault scarp  
225 by the mean of HR bathymetry highlighting a 3 km-long, up to 0.9 m-high scarp, but  
226 concluded that part of the observed slip may be post-seismic. The Les Saintes earthquake  
227 generated up to 2 m-high tsunami waves at the coast and a maximum horizontal run-up  
228 of 42 m in some bays of Les Saintes (Zahibo et al., 2005; Le Friant et al., 2008; Cordrie et

229 al., 2020). However, tsunami models using fault parameters based on seismological data  
230 resulted in an under-estimation of the tsunami wave amplitude and run-up (Le Friant et  
231 al., 2008). Cordrie et al. (2020) consider that their best fit models require greater slip on  
232 the fault plane and a greater magnitude for the earthquake than those given by the  
233 seismological data in order to accurately reproduce the observed tsunami, suggesting  
234 that the observed scarp is the surface expression of co-seismic slip (source parameters:  
235  $M_w, M_w=6.4-6.5$  – fault plane 15x15 km – Strike N325°E – Dip 55°E – rake ca.90° - slip=2.5-  
236 3.5 m).

237 Over the last ~500 years of historical written archives in the Lesser Antilles, a few  
238 dozen confirmed tsunamis from different origins (local, regional or far-field sources  
239 including earthquakes, landslides, volcanic eruptions or combinations of them) have  
240 been reported. Starting with the 16 April 1690 Ms~8.0 Barbados earthquake (which  
241 presumably triggered the first reported tsunami in the Lesser Antilles), it includes the  
242 widely studied 1 November 1755 Lisbon transoceanic tsunami (*e.g.*, Gutscher et al., 2006,  
243 Accary and Roger, 2010; Roger et al., 2010, 2011, Martinez-Lorient et al., 2021) and the  
244 18 November 1867 Virgin Islands tsunami (*e.g.*, Zahibo et al., 2003, 2005; Barkan and ten  
245 Brink, 2004). Landslide sources and/or pyroclastic flows, are also known for their  
246 tsunamigenic potential. There are more and more studies led to assess the hazard  
247 associated to these “silent tsunamis” (*e.g.*, Roger et al., 2024). In the Caribbean Region, a  
248 few tsunamis triggered by landslides and/or pyroclastic flows have been reported in  
249 catalogues of events (*e.g.*, O’loughlin and Lander, 2003; Accary and Roger, 2010),  
250 bathymetric surveys helped to identified large submarine landslide scars and deposits  
251 (*e.g.*, Deplus et al., 2001; Le Friant et al., 2009, 2019) and a few studies have highlighted  
252 the capacity of these landslides to trigger large tsunamis (*e.g.*, Smith and Shepherd, 1996;  
253 Teeuw et al., 2009; Leslie and Mann, 2016).

254 On the basis of an extensive literature review, including cross-checking of  
255 information, we conclude that only four tsunamis reported in Guadeloupe are likely of  
256 upper crustal seismic origin (Mallet, 1853, 1854, 1855; Lander, 1997; Zahibo and  
257 Pelinovsky, 2001; Lander et al., 2003; O’Loughlin and Lander, 2003; Zahibo et al., 2003;  
258 Accary and Roger, 2010; Nikolkina et al., 2010; Roger et al., 2013; online databases:  
259 NGDC/WDS, 2023; TL/ICMMG, 2023). These tsunamis have been observed or recorded  
260 following earthquakes occurring on regional faults (indicated magnitude and epicenter  
261 coordinates are from the USGS online earthquakes catalogue;



262 <https://www.usgs.gov/programs/earthquake-hazards>): the  $M_w$   $M_w \sim 8.0-8.5$  earthquake  
263 on 8 February 1843 (NE of Guadeloupe, 16.73°N, 61.17°W) and the  $M_w$   $M_w 7.2$  earthquake  
264 on 25 December 1969 (SE of Guadeloupe, 15.648°N, 59.694°W) are arguably attributed  
265 either to a rupture along the megathrust or to upper plate faulting ; the  $M_w$   $M_w 6.5$   
266 earthquake on 16 March 1985 (along the Harvers-Montserrat-Bouillante fault system  
267 between Montserrat and Nevis, north of Basse-Terre, 17.013°N, 62.448°W); and the  
268  $M_w$   $M_w 6.3$  earthquake on 21 November 2004 (Along the Les Saintes fault system, south  
269 of Basse-Terre, 15.679°N, 61.706°W)(Figure-1). The largest earthquakes and tsunamis  
270 produced at subduction zones are expected to originate from rupture at the plate  
271 interface megathrust. However, historical records in the Lesser Antilles reveal that  
272 neither the 1843  $M_w$  7.5-8.5 nor the 1839  $M_w$  7.5-8.5 largest known earthquakes,  
273 although destructive, have been followed by large tsunamis. However, Roger et al. (2013)  
274 showed that the simulation of a  $M_w$  8.5 1843-like megathrust earthquake would have  
275 produced wave amplitudes of 5 m and more along the exposed coasts of Guadeloupe,  
276 which was not reported in coeval documents. Feuillet et al. (2011) explain these two  
277 major earthquakes by the great depth of the rupture along the megathrust that led to little  
278 seafloor deformation. However, numerical simulation of worst-case scenarios for these  
279 two ruptures along the megathrust evidence the possibilities of tsunami amplitudes up  
280 to 10 meters and above in some embayment (Roger et al., 2013; Colon-Useche et al., 2023.  
281 As magnitude of crustal earthquakes is constrained by fault length, events occurring  
282 along such crustal fault show a much smaller magnitude than megathrust earthquakes  
283 ~~but consequently they~~ may form ~~smaller large~~ seafloor offsets. Thus, most crustal  
284 earthquakes able to trigger a tsunami do not produce significant sea surface deformation  
285 (only a few centimeters amplitude in most cases) compared to subduction interface  
286 earthquakes. Associated tsunamis are typically only visible on pressure gauge records  
287 (coastal gauges or DART ~~stations~~ systems) after processing the data (*e.g.*, de-tiding, high-  
288 frequencies filtering, etc.).

### 290 **3. Material and method**

#### 292 **3.1 Seismic lines**

293 We present eight multichannel seismic (MCS) lines acquired during five  
294 oceanographic campaigns (location on Figure 3A). These include high-resolution sparker  
295 source seismic data from KaShallow 1 (Lebrun et al., 2009) and GEOBERYX03  
296 oceanographic campaigns (Thinon and Bitri, 2003; Thinon et al., 2004 and 2010), mid  
297 resolution GI airgun arrays seismic data from KaShallow 2 (Lebrun et al., 2009) and  
298 Aguadomar (Deplus et al., 1999) cruises, and deep penetrating MCS data from the  
299 Sismantilles 1 seismic experiment (Hirn, 2001) (Table 1).

300 Sismantilles 1 seismic data have been processed using CGG-Veritas Geovector®  
301 software on board the R/V Nadir (Hirn et al., 2001). Processing includes band pass  
302 filtering, internal and external mute, one step velocity analysis, NMO correction, stack,  
303 predictive deconvolution and post-stack constant water-velocity time migration. The  
304 KaShallow 1 and 2, Aguadomar and Geoberyx have been processed with Seismic Unix  
305 software ([Cohen and Stokwell, Center for Wave Phenomena, Colorado School of Mines](#)).  
306 The seismic processing includes band pass filtering, sea waves and spherical divergence  
307 corrections, constant velocity or simple velocity gradient NMO correction and stack, and  
308 constant water-velocity time migration. The reflection seismic lines are in millisecond  
309 two-way-travel-time (mstwt). The velocities of the Wide Angle Seismic refraction (WAS)  
310 profiles are in second two-way-travel-time (stwt).

311

### 312 *3.2 Bathymetry*

313 High-resolution bathymetric data were acquired during the KaShallow2  
314 oceanographic campaign (Lebrun, 2009) using ~~the a~~ Simrad EM300 multibeam  
315 echosounder. We merged this data with Aguadomar (Deplus, 1999) and Sismantilles 2  
316 (Laigle et al., 2007) cruises Simrad EM12 Dual multibeam echosounder data available for  
317 the Marie-Galante Basin. Vertical accuracy for these echosounders is plurimetric for  
318 typical water depth found in the Marie-Galante Basin (<2000 m below [mean](#) sea-level,  
319 noted bsl hereafter). Near-shore (0-200 m bsl) and onshore, very high-resolution  
320 bathymetric and topographic data comes from the Litto3D database -  
321 (<https://www.geoportail.gouv.fr/donnees/litto3d> last accessed on September  
322 ~~2020~~2024- that includes airborne lidar survey and KaShallow-3 multibeam data  
323 acquired with a RESON Seabat 8101 multibeam echosounder). The vertical accuracy for  
324 this second dataset is better than one meter. We used [the Caraibes software \(ifremer\)](#) to  
325 process the data and to produce a 25 m grid spacing Digital Elevation Model of the Marie-

326 Galante Basin and surrounding islands. Maps are produced using the open-access QGIS  
327 software (<https://www.qgis.org>)

328

### 329 *3.3 Depth and time calibration of main geological boundaries.*

330 In order to measure offsets of unconformities on time-migrated seismic lines we  
331 need to constrain the seismic velocities within the sediments. We used velocities from the  
332 WAS profile (Kopp et al., 2011) in the south of Marie-Galante, that trends parallel to the  
333 MCS line Agua116 (Cornée et al., 2023). The WAS velocities in the *ca.* 0.4 stwt (second  
334 two way time) thick upper unit (MG-MS3 – Cornée et al., 2023) ranges between 2 and 2.5  
335 km/s. The 3.25 km/s isochrones mimic the base of unit MG-MS2 and the 4.5 km/s  
336 isochrones follow the acoustic basement below MG-MS1. Moreover, ~~KaShallow~~  
337 KaShallow 2 cruise MCS data (Table 1) acquired with a 600 m long streamer allows us to  
338 determine the Normal Move Out velocities down to a depth of *ca.* 0.75 stwt in well-  
339 layered units such as shown on the seismic lines (Figure 3). Once converted into interval  
340 velocities using the “Hewitt Dix formula”, we determine velocities in the upper unit from  
341 1500 to 2750 m/s (Dix, 1955). Therefore, we use 1500 m/s in the water and 2000 m/s  
342 and 2500 m/s in the sediments to estimate (and bound) the depth of unconformities  
343 observed on time-migrated seismic lines (Table 2).

344 Offshore, several first order unconformities and sedimentary units were  
345 accurately dated using bio-stratigraphy analysis or radiochronology (Bouysse and  
346 Mascle, 1994; KaShallow Research Program results: ~~Cornée et al., 2023; De Min, 2014;~~  
347 ~~De Min et al., 2015;~~ Münch et al., 2013; De Min, 2014; De Min et al., 2015; Cornée et al.,  
348 2023). The deepest dated unconformity, MG-SB2, which corresponds to the top of the  
349 MG-MS1 sequence, occurs on seismic lines east of Marie-Galante (thick orange line on  
350 Figure 5, lines AGUA97 – K09-09 – K09\_45 - Sis7C). Along the seismic line Agua 97, the  
351 F8 fault scarp has been sampled at 514 m bsl just beneath the unconformity (KaShallow  
352 Cruise ROV dive, Figure 6). The samples, BMG2 and 4, yielded a Late Burdigalian/earliest  
353 Langhian age (Cornée et al., 2023). Thus, we propose 16 Ma ± 1Ma for the age of MG-SB2.  
354 Above, another regional unconformity MG-SB3 (Cornée et al., 2023) is identified east of  
355 Marie-Galante. It corresponds to the top of MG-MS2 sequence (thick purple line on the  
356 Figure 5 lines Agua97 – K09-09-08 – K09-45-44 – Sis7C). The age for this surface is  
357 bracketed between the overlying Late Messinian GT carbonate platform (zones N18, 5.8-  
358 5.33 Ma –Cornée et al., 2023) and the underlying sedimentary unit dated Late Tortonian

359 8.57 ± 0.43 Ma (Ar-Ar, Münch et al., 2014). We thus consider 7 ± 1.5 Ma for the age of MG-  
360 SB3. West of Marie-Galante, the angular unconformity on line K09-90 North-West of  
361 Marie-Galante may corresponds to MG-SB3 (Figure 4). However, this reflector is too deep  
362 to be followed across the whole fault system. Within the uppermost sequence, MG-MS3,  
363 a remarkable unit boundary corresponding to a second order unconformity, can be easily  
364 correlated throughout the basin and onshore (red thick line on Figure 4). This unit  
365 boundary is Middle-Late Piazencian offshore and correlates onshore with the 3–2.9 Ma  
366 tectonically-induced erosional unconformity SB1 (see above; Cornée et al., 2023). Along  
367 the seismic line Ber03-30-31, the fault scarp immediately north of F3 and F4 has been  
368 sampled at 283 m bsl (KaShallow Cruise ROV dive, Figure 4). Samples, BC1 and BC2,  
369 yielded ages of 1.33 ± 0.23 Ma and 1.15. ± 0.12 Ma, respectively (Ar<sup>40</sup>/Ar<sup>39</sup> ages on  
370 plagioclases, Münch et al., 2013; 2014). These samples correspond to a prominent seismic  
371 reflector within the upper unit of MG-MS3 sequence that can also be easily correlated  
372 through all the seismic lines west of Marie-Galante. We thus retain an average age of 1.29  
373 ± 0.26 Ma for this seismic reflector (green line on Figure 4).

374

### 375 *3.4 Tsunami modeling*

376 In order to test the tsunamigenic potential of the different-fault system proposed  
377 faults herein, several-a rupture scenarios have-has been elaborated and are-is presented  
378 hereafter.

379 Numerical simulations of tsunami generation and propagation were carried out  
380 using COMCOT software (Cornell Multi-grid Coupled Tsunami: Liu et al., 1998; Wang,  
381 2008; Wang and Power, 2011). COMCOT is widely used by the research community and  
382 constantly tested notably through various real tsunami cases (e.g. Prasetya et al., 2011;  
383 Gusman et al., 2019; Paris et al., 2021; Gusman et al., 2022; Roger et al., 2023). COMCOT  
384 uses a modified staggered finite-difference scheme to solve linear and non-linear shallow  
385 water equations in either spherical or Cartesian coordinate systems throughout a set of  
386 nested grids allowing refinement of the bathymetric resolution in coastal areas. A two-  
387 way nested grid configuration is implemented in the model to balance computational  
388 efficiency and numerical accuracy (Wang 2008; Wang and Power 2011).

389 For this study, nesting has been used with two grid levels: the first grid is a 0.5  
390 arcmin (~900 m) resolution grid of the Lesser Antilles (extent: 295°E, 302°E, 12°S, 18°S)  
391 built from the global dataset GEBCO 2021 (GEBCO Compilation Group, 2021); the second

392 grid is a 3.75 arcsec (~115 m) spatial resolution grid focusing on the Guadeloupe  
393 Archipelago and Dominica Island, including the location of the investigated Morne Piton  
394 ~~faults-location system~~ as shown on Figure 1 (extent: 297.92°E, 300.22°E, 14.94°N,  
395 16.717°N). This second grid has been built from different datasets including the  
396 aforementioned bathymetric data (§ 3.2). The highest resolution and the ~~more-most~~  
397 recent data have been kept first. Data gaps have been filled in with data from GEBCO 2021  
398 (GEBCO Compilation Group, 2021) for offshore regions, and SRTM version 3.0 Global 1  
399 arc-second data (NASA SRTM, 2013) for onshore regions. Continuity of the different  
400 datasets has been ensured using kriging interpolation, which has proven to be one of the  
401 best methods ~~to apply in order~~ to produce a well-defined DEM, especially for smooth  
402 transitions between different resolution areas (e.g. Bernardes et al., 2006; Arun, 2013;  
403 Ajvazi and Czimber, 2019). Note that Dominica was included in the second grid ~~was-in~~  
404 order to look at potential effects which could occur between the different islands and also  
405 to assess the potential tsunami threat resulting from the Morne Piton scenario on this  
406 neighboring island.

407 The initial sea-bottom displacement ~~of every simulation~~ is calculated by COMCOT  
408 considering an instantaneous rupture of the fault using ~~Okada (1985)'s rupture~~the  
409 surface deformation model of Okada (1985), and transmission of the deformation to the  
410 water column above is considered instantaneous. Calculations of wave propagation have  
411 been done at mean sea level (MSL) assuming a constant Manning's roughness coefficient  
412 of 0.011 for the seabed friction (Wang et al., 2017). A higher friction coefficient leads to  
413 more energy dissipation of tsunami waves, especially in shallow waters, slowing down  
414 their speed and reducing their amplitude and impact (e.g. Dao and Tkalich, 2007).  
415 Considering the limited extent of the interest zone (~250km x 200km), the rupture  
416 parameters (leading to a small coseismic rupture) and the objective to look at potential  
417 localized effect as inter-islands resonance, tsunami waves propagation time was set to 10  
418 hours.

419

## 420 **4. RESULTS**

421

### 422 *4.1 The Morne Piton ~~f~~Fault system*

423 The HR bathymetric data presented here above (section 3.2) allows to refine the  
424 structural pattern of the Morne Piton ~~f~~Fault system, especially offshore (Figures 3A - B).

425 The fault system splays eastward from the N120-N135°E trending Eastern Les Saintes  
426 fault system located east-south-east of Basse-Terre to the N110-115°E trending Petite-  
427 Terre fault system south-south-east of Grande-Terre (Figures 2 and 3). Thus, the fault  
428 zone spreads over a 5-8 km wide and 50 km long zone with an average N100°E trend.

429 Morpho-bathymetric analysis allows us to identify surficial segments of the faults  
430 that are reaching out the seafloor. The main fault scarp of the Morne Piton fault system is  
431 the southernmost one, along which 9–11 fault segments of 1-10 km length can be  
432 identified (Figure 3B). From west to east, the F1 segment trends N110° and then the fault  
433 steps left along the N75°E trending F2 segment. A little farther east, the fault cuts the  
434 northern Colombie Bank and the eastern Marie-Galante platform along closely spaced  
435 N90°E trending left or right stepping segments F3, F3', F4 and F5. Across the island, the F6  
436 segment is a N130°N trending, 6 km long right step relay linking the F5 segment to the F7  
437 N90°E trending one. Further east offshore Marie-Galante, two N80°E trending fault  
438 segments, F8, and F9, 10 and 11, arrange as overlap right steps. There, the fault scarp  
439 vanishes in just a few kilometers. To the east of the line Sis7C, neither the sediments nor  
440 the basement are affected by the north-dipping Morne Piton fFault system (Figure 5). In  
441 contrast, the seismic line Sis7C shows that the basement is southwardly downthrown by  
442 the Petite-Terre fault system, along south dipping active and sealed faults to the north  
443 and south of the Morne Piton fFault system, respectively (Figure 5 location on Figure 3A)  
444 . West of Marie-Galante, the Morne Piton fFault system widens as closely spaced fault  
445 splays trending N95°E to N100°E link the main fault scarp (F2, F3 and F4) to the antithetic  
446 Goyave Fault system or die westward (Figure 4 location on Figure 3A). Eastward of the  
447 F6 segment, some synthetic and a few antithetic faults splay northeastward and link with  
448 the N110-115°E Petite-Terre Fault system.

449 The mean fault-scarp height west of Marie-Galante Island is ca. 100 m (Figure 3C).  
450 Across Marie-Galante Island, the mean fault-scarp height reaches 200 m and controls the  
451 staircase morphology of the island. East of the island, the Marie-Galante Canyon carved  
452 the sedimentary units, clearing some of the fault planes increasing their apparent scarps  
453 heights up to 400 m. To the east, the canyon meanders and cuts through the eastern tip  
454 of the Morne Piton Fault fault system (Figure 3 B and C). West of the island, at the vicinity  
455 of the volcanic island of Basse-—Terre, either recent deposits or the uppermost  
456 sedimentary units seal most of the faults. These observations seem to indicate that the

457 sedimentary rate west of Marie-Galante and the erosional rate east of Marie-Galante (in  
458 the canyon) exceed the vertical slip rate of the fault.

#### 459 4.2 Vertical slip rate estimates along the Morne Piton ~~f~~Fault system

460 To assess the average vertical slip rate along the Morne Piton ~~f~~Fault system, we  
461 estimated the fault offset of key dated reflectors across the entire length of the fault  
462 system (Figures 4 and 5 – Table 2). West of Marie-Galante, the main offset of the  $1.29 \pm$   
463  $0.26$  Ma seismic reflector (green on Figure 4) increases from west to east (i.e., from the  
464 westernmost extremity of the fault toward its center). Close to the eastern shore of Basse-  
465 Terre Island (Figure 4, profile K09-96, and Table 1), the 1.29 Ma reflector is downthrown  
466 by 110-115 m. Eastward, the reflector offset increases up to 230-257 m (Figure 4, line  
467 K09-90, K08\_24 and Table 2) and reaches a maximum of 300-322 m (Figure 4, lines  
468 ber03\_30-31, K08-59). Accordingly, the number of sealed structures across the fault  
469 system decreases eastward (Figures 3 and 4). Thus, West of Marie-Galante, the Morne  
470 Piton ~~f~~Fault system accommodates a vertical slip rate increasing eastward up to  $0.25 \pm$   
471  $0.08$  ~~mm·yr~~<sup>mm·yr<sup>-1</sup></sup> over the last  $1.29 \pm 0.26$  Ma (Table 2).

472 The  $2.95 \pm 0.05$  Ma Unit Boundary (red line on figure 4) can only be correlated  
473 across the fault system along the K08-59 seismic line. Growth strata are observed in the  
474 deposits above the 2.95 Ma unit boundary (Figure 4, gray shadow on seismic lines),  
475 attesting for syn-sedimentary fault activity. This unit boundary offset reaches 550-620 m,  
476 leading to  $0.20 \pm 0.02$  ~~mm·yr~~<sup>mm·yr<sup>-1</sup></sup> average vertical slip rate over the last  $2.95 \pm 0.05$   
477 Ma, i.e. ca.  $0.16$  mm·yr<sup>-1</sup> for the period 2,95 - 1,29Ma (Table 2). West of Marie-Galante  
478 island, deeper reflectors cannot be identified and correlated across the fault system  
479 because of the limited seismic penetration. These two estimates are compatible within  
480 their uncertainties and suggest a steady slip rate of the Morne Piton Fault since ca. 3 Ma  
481 at least.

482 ~~But~~However, ~~E~~east of Marie-Galante, the MG-SB2 sequence boundary dated to  $16$   
483  $\pm 1$ Ma (orange in Figure 5 – see also Figure 5 in Cornée et al., 2023) is the only reflector  
484 that can be correlated on both sides of the fault system. In the hanging wall of the fault,  
485 the younger MG-SB3  $7 \pm 1.5$ Ma boundary (Purple in Figure 5) as well as a large part of  
486 the fault scarp are eroded by the Marie-Galante Canyon. The seismic line K09-09 (Figure  
487 5) shows that the MG-SB3 unconformity records the Morne Piton ~~f~~Fault inception: in the  
488 footwall of the fault, the stratigraphy of MG-MS2 sequence (comprised between MG-SB2

489 and MG-SB3) shows conformal deposits flexed upward while approaching the fault,  
 490 whereas MG-MS3 deposits onlap onto MG-SB3 and present clear growth strata. We thus  
 491 propose that the  $16 \pm 1$  Ma sequence boundary is pre-tectonic and is tilted by the fault  
 492 since its inception  $7 \pm 1.5$  Ma ago (the age of MG-SB3; Figure 5, profile K09-45-45). Along  
 493 the fault system East of Marie-Galante we calculated the strain rate from MG-SB2 offset  
 494 since  $7 \pm 1$  Ma. From east to west the slip rate ranges from  $0.067 \pm 0.03$   $\text{mm}\cdot\text{yr}^{-1}$  at  
 495 the K09\_44-45 seismic line, to  $0.071 \pm 0.02$   $\text{mm}\cdot\text{yr}^{-1}$  along the K09\_08-09 line.  
 496 Seismic line Agua97 (Figure 5) presents the greatest offset of MG-SB2. However, this  
 497 seismic line does not cross the southernmost F7 segment (the water depth is too shallow  
 498 for ship navigation in the footwall compartment). We estimated the depth of MG-SB2 in  
 499 the footwall compartment from the closest seismic line available that crosses the fault  
 500 located 1 km east of the Agua97 line. We obtain an offset of ~~830977-860995~~ m leading to  
 501 a maximum average vertical slip rate of  $0.125 \pm 0.035$   $\text{mm}\cdot\text{yr}^{-1}$  since  $7 \pm 1.5$  Ma,  
 502 i.e. ca.  $0.07$   $\text{mm}\cdot\text{yr}^{-1}$  for the period 7 - 2,95Ma (Table 2). Consequently, we propose that i)  
 503 the vertical slip rate accommodated by the Morne Piton ~~f~~Fault system increases  
 504 progressively from each extremity of the fault toward its center, and ii) that the Morne  
 505 Piton ~~f~~Fault system is characterized by ~~a constant an increasing~~ slip rate of from ca.  $0.07$   
 506 from its inception (i.e. 7 Ma ago) to ca.  $0.250 \pm 0.05$   $\text{mm}\cdot\text{yr}^{-1}$  since its inception  
 507 since 1.29 Ma (Table 2), i.e. 7 Ma ago.

#### 508 *4.3 Earthquakes parameters of Tsunami modeling*

509 ROV dive along the ber03\_30-32 seismic line allowed observation of one of the main  
 510 morphologic scarps of the Morne Piton ~~f~~Fault system across the F2 and F3' segments  
 511 (Figures 3 and 6). Across the upper plateau, between F2 and F3', we observed several  
 512 N90°E trending fractures parallel to the fault segments (Figure 6A). While descending  
 513 across the F3' scarp, the slope progressively steepens up from  $45^\circ$  at 157 m bsl to more  
 514 than  $80^\circ$  at 280 m bsl just a few meters above the toe of the scarp (Figure 6A, B and C).  
 515 This morphology suggests a ca. 128 m-high cumulative scarp for the F3' segment at that  
 516 location. The very last meter of the fault scarp above the toe of the slope presents a 100  
 517 cm-high polished vertical surface, partly altered, showing dip-slip striations indicating  
 518 pure normal motion along this fault segment (Figure 5D E and F). This exposed and partly  
 519 altered fault slip plane breaches the sea floor at high angle. Such a polished striated fault  
 520 scarp morphology is similar, although more altered, to the co-seismic fault scarp



521 observed at the toe of the Roseau Fault plane, after the Les Saintes earthquake (Escartin  
522 et al., 2016). We conclude that this observation of the Morne Piton polished striated scarp  
523 may correspond to one of the last co-seismic scarps formed during a major earthquake  
524 (including possible post-co-seismic slip motion) along this fault. Alteration of the fault  
525 slip plane suggests that the slip event occurred tens to several hundred years ago, *i.e.*, this  
526 fault slip plane may correspond to a pre-instrumental earthquake (see discussion). From  
527 this observed scarp we obtained a ratio of last event scarp over total scarp height (proxy  
528 for the cumulative slip as determined on Figure 3) of ~2,6%. With this ratio we calculated  
529 an average scarp of ~75 cm along the whole length of the fault and a maximum scarp of  
530 2 m. Such an average scarp value corresponds to the surface expression of a magnitude  
531  $M_w$  ~6.75 earthquake using the criteria of Wells and Coppersmith (1994), Leonard  
532 (2010) or even 7 according to Thingbaijam et al. (2017). The same studies also provide  
533 a calculated maximum displacement of ~2m, consistent with the maximum observation  
534 along the scarp. Moreover, the 45 km total length of the Morne Piton Fault system  
535 measured from HR bathymetry, together with the width of the fault given by the 10 to 15  
536 km thick seismogenic crust, lead to a rupture area ranging between ~ 450 to 675 km<sup>2</sup> that  
537 would generate a magnitude  $M_w$  ~6.75 ± 0.15 earthquake corroborating the afore  
538 range of magnitude deduced with other observations (e.g.,  $M_w$  ranging between 6.6 and  
539 6.8 according to Wells and Coppersmith, (1994) and; Leonard (2010) and around 7  
540 according to; Thingbaijam et al., 2017). The rupture parameters for the different  
541 identified segments of the fault shown on figure 3B are provided in Table 3. Geographic  
542 location of the center of top of the fault plane and azimuth are provided based on our  
543 structural analysis (section 4.1 and 4.3). Neither seismic lines which illustrate only a few  
544 hundred of meters nor in-depth earthquake distributions (which is not enough resolved)  
545 allow to estimate the dip of the Morne Piton Fault system. Thus, after showing  
546 that considering the influence of dip on surface deformation which turns out to be is  
547 neglectable, we choose a mean dip of 75° for the fault segments after Feuillet et al.  
548 (2004). The shape of the rupture area (along-strike length x downdip width) and a slip of  
549 1.89 m (maximum displacement estimated from scarp height measurement) is  
550 implemented for each segment in order to fit with a total fault surface of ca. 500 km<sup>2</sup>,  
551 corresponding to a magnitude  $M_w$  6.5 earthquake. Finally, conformably to pure dip  
552 slip striations observed along the F3' segment (section 4.3) and the F7 segment (Feuillet  
553 et al. 2002), we apply a rake of 90°, corresponding to a pure normal faulting mechanism

554 as observed by Feuillet et al. (2004) at Anse Piton and by the ROV picture of the present  
555 study}. Fault segments F8 and F9 are not straight, for the purpose of modeling they have  
556 been divided into F8-F98' and F109-F119' (Figure 7).

557 Hereafter, we use these parameters to evaluate the potential tsunami hazard from the  
558 Morne Piton ~~f~~Fault for a worst-case plausible scenario rupturing all the segments  
559 simultaneously.

#### 560 561 4.4 Plausible worst-case tsunami scenario and resulting 562 hazard~~Related tsunami hazard~~

563  
564 We present a worst-case plausible scenario, related to a rupture along all the  
565 identified segments of the Morne Piton ~~f~~Fault system as these 1 to 10 km-long segments  
566 most probably root in-depth along a single fault zone (Feuillet et al., 2004). We rule out  
567 the eventuality of testing a single 10 km-long segment of the Morne Piton ~~f~~Fault system  
568 rupture as it would generate a  $M_w < 6.0$  earthquake and would thus unlikely consist in  
569 a tsunami source (e.g., Roger et al., 2019). Here, we use a ~~maximum~~ plausible  $M_w$  6.5  
570 scenario, i.e a magnitude slightly lower than the maximum magnitude  $M_w$  6.7 deduced  
571 from the morphological analysis, but closer enough to the Les Saintes earthquakes  
572 magnitude as both Les Saintes and Morne Piton ~~f~~Fault systems share close  
573 morphological characteristics. ~~that Our model~~ would generate a tsunami with a  
574 significant energy/amplitude to accurately highlight the potential consequences of  
575 tsunami waves' propagation and interaction with the peculiar shallow reliefs and major  
576 embayment located in and around the Marie-Galante Basin. Quantifying horizontal run-  
577 up at the coast and assessing tsunami risk following a rupture along this fault is out of the  
578 scope of the present study as such quantifications necessitate a better knowledge of the  
579 fault dynamic itself (return period of large events, etc.).

580 ~~The rupture parameters for the different identified segments of the fault shown on~~  
581 ~~figure 3B are provided in Table 3. Geographic location of the center of the fault plane and~~  
582 ~~azimuth are provided based on our structural analysis (section 4.1 and 4.3). Neither~~  
583 ~~seismic lines which illustrate only a few hundred of meters nor in depth earthquake~~  
584 ~~distributions (which is not enough resolved) allow to estimate the dip of the Morne Piton~~  
585 ~~Fault system. Thus, after showing that the influence of dip on surface deformation is~~  
586 ~~neglectable we choose a mean dip of  $75^\circ$  for the fault segments after Feuillet et al. (2004).~~

~~The shape of the rupture area (along strike length x downdip width) and a slip of 1.89 m is implemented for each segment in order to fit with a total fault surface of ca. 500 km<sup>2</sup>, corresponding to a magnitude Mw 6.5 earthquake. Finally, conformably to pure dip slip striations observed along the F3' segment (section 4.3) and the F7 segment (Feuillet et al., 2002), we apply a rake of 90° (pure normal faulting mechanism as observed by Feuillet et al., 2004 at Anse Piton and by the ROV picture of the present study). Fault segments F8 and F9 are not straight, for the purpose of modeling they have been divided into F8-F8' and F9-F9'.~~

— The initial surface elevation directly resulting from the Okada (1985)'s formulation is ~~indicated~~ presented in Figure 7. Due to the high inclination of the fault planes (dip = 75°) dipping globally ~~southward~~ northward, a profile cut of the initial displacement is represented from the north to the south by a crest (positive elevation) and a trough (negative elevation). At t=0, the shallow water equations take over from this initial deformation and the propagation of the tsunami waves is calculated over the nested grids at adequate time steps. Figure 8 presents the state of the virtual water surface at six different times of the tsunami waves propagation from 1 to 16 minutes. The wave front initially parallel to the fault axes (t ≤ 1 min) is progressively influenced by the bathymetry within the very first minutes following the rupture, leading to an anisotropic propagation of the waves showing variability in space and time. In addition, the fact that the fault literally crosses Marie-Galante leads to the tsunami source being divided in two independent sources located on the west and east of this island: two tsunamis are therefore generated and called TsuW (on the west) and TsuE (on the east) hereafter. These two tsunamis propagate from their origin and wrap around Marie-Galante as shown at t=4 min of propagation. Then, between 4 and 9 min, the two tsunami fronts meet on the north and south of Marie-Galante. Meanwhile, the propagation of the TsuW waves meet the shallow waters of the Banc Colombie shoal (approx. coordinates: 15.98°N/-61.43°W; minimum water depth ~~of less than is about 3550m~~), west of Marie-Galante: the waves' amplitude increases as they slow down and their interaction leads to a constructive interference resulting in a "new" tsunami source at the Banc Colombie shoal, mainly showing a negative wave propagating southward with some extensions toward Marie-Galante on the east and Les Saintes on the west. ~~This relatively high amplitude negative wave is shown by VG\_1 on figure 10 with a peak to trough value of ~0.6 m. VG\_2 and VG\_3 also show it to a lesser extent a bit later.~~

620 Approaching the coasts, wave shoaling takes over, the reduction in water depth  
621 slowing down the waves and simultaneously increasing their amplitude. It leads to wave  
622 amplification as particularly shown along Marie-Galante north shore, the southeast coast  
623 of Basse-Terre and the south of Petite-Terre and/ eastern Grande--Terre (Figure 9).

624 After 10 hours of tsunami propagation, the maximum values of wave amplitude  
625 reached on each point of the simulation domain are shown in Figure 9. The overall impact  
626 of such an event is that the maximum wave amplitude is not going over 1.2 m, carefully  
627 considering the 100 m resolution of the simulation domain: in fact, grid a-refinement at  
628 the coast showing higher resolution ~~grid~~-would probably ~~highlight~~show higher wave  
629 amplitude in very localized areas because of interaction with small underwater  
630 structures not represented at this resolution, and-as well as non-linear effects. The  
631 patterns of those amplitudes indicate that not only the fault region but also some coastal  
632 regions are exposed to tsunami waves of 50 cm or more, which is above the usual beach  
633 and marine threat 30-cm threshold. It is the case for the neighboring coasts of Marie-  
634 Galante, southeast Basse-Terre, south Grande-Terre and the natural reserve of Petite-  
635 Terre. The southeast coast of Basse-Terre is particularly exposed with ~~waves-wave~~  
636 amplitudes of more than 1 m (Figure 9a). A focus on Les Saintes Archipelago highlights  
637 also wave amplitudes of more than 1 m, even between the islands (Figure 9b). The  
638 northeast coast of Dominica is also affected but to a lesser extent (maximum wave  
639 amplitudes of ~50 cm). Further high-resolution simulation, including flow speed  
640 calculations, would help to correctly assess the related hazard on this island. Virtual sea-  
641 level gauges have been added at different locations of grid 2 (Figure 9) -in order to check  
642 if the model is stable and to look for possible resonance (especially in Les Saintes  
643 Archipelago). The raw signal of seven VG (top figure 10) highlights a clear decrease of the  
644 amplitude over the time on all stations. However, for stations VG\_1, VG\_2 and VG\_3, a low-  
645 frequency oscillation is clearly visible and lasts for at least 10 hours. The amplitude  
646 spectrums on these three stations show that two peaks with a period of ~~~86.5 min~~  
647 17-15 min respectively are present on the three signals at Les Saintes, which is not the  
648 case for the stations out of the archipelago. Moreover, the high amplitude negative wave  
649 southwardly propagating generated by the "new" tsunami source at the Banc Colombie  
650 shoal, is shown by VG 1 on figure 10 with a peak to trough value of ~0.6 m. VG 2 and  
651 VG 3 also show it to a lesser extent a bit later.

652

## 5. Discussion

### 5.1. Upper plate fault tsunamigenic potential. Implications a local and regional scales

~~The highest largest magnitude earthquakes and strongest tsunamis produced at subduction zones are expected to originate from rupture at the plate interface megathrust. However, historical records in the Lesser Antilles reveal that neither the 1843 Mw 7.5-8.5 nor the 1839 Mw 7.5-8.5 largest known earthquakes, although destructive, have been followed by large tsunamis. However, Roger et al. (2013) showed that the simulation of a Mw 8.5 1843-like megathrust earthquake would have produced wave amplitudes of 5 m and more along the exposed coasts of Guadeloupe, which was not reported in coeval documents. Feuillet et al. (2011) explain these two major earthquakes by the great depth of the rupture along the megathrust that lead to little seafloor deformation. However, numerical simulation of worst-case scenarios for these two ruptures along the megathrust evidence the possibilities of tsunami amplitudes up to 10 meters and above in some embayment (Roger et al., 2013; Colon-Useche et al., 2023). OUI JE PENSE QU'ON PEUT SUPPRIMER CA.~~

Les Saintes earthquake demonstrated that upper plate normal faults may generate  $M_w > 6$  tsunamigenic earthquakes in the Lesser Antilles. Les Saintes tsunami produced up to 2 m high waves at the coast and 42 m distance run-up in a peculiar embayment (Cordrie-Zahibo et al. 200205). Such normal faults are prone to be tsunamigenic because their rupture is relatively shallow (compared to the megathrust), and their slip motion is favorable to large seafloor displacement. Together with their proximity to the islands, they are able to produce metric-high tsunami waves at the coast and tens to hundreds of meters of run up distances (depending on the topography). Therefore, upper plate crustal faults may represent a major potential tsunami hazard in the Lesser Antilles islands and particularly in the Guadeloupe Archipelago as pointed out by the Intergovernmental Oceanographic Commission held in Fort-de-France in 2019 (IOC-UNESCO, 2020). Similarly to Les Saintes Fault, we assume that the 50 km long Morne Piton fault poses a potential earthquake and tsunami hazard. The large scarp we observed at the toe of the Morne Piton fault suggests recent tsunamigenic seismogenic rupture(s) along this structure, potentially tsunamigenic. However, this scarp might not be related to the 1851 historical event as the estimated magnitude  $M_w$  5-5.5 for this earthquake appears too

low to explain the observed scarp. Thus, a rupture of the fault along its whole length must not be excluded. Several other prominent onshore-offshore faults affect the seafloor and the topography of the archipelago and may represent both an earthquake and a tsunami hazard. However, the relationships between faults, earthquakes and tsunami is not clearly established as shown in the following examples.

Along the arc, the Harvers-Montserrat-Bouillante and Les Saintes fault systems are the most prominent tectonic features (Feuillet et al., 2010). To the south, Les Saintes Fault system dips east and defines a half-graben (Leclerc et al., 2016). The westernmost fault, the Roseau fault, ruptured during the 2004  $M_w$  6.3 earthquake and is most ~~probably~~ ~~now~~ likely reloading stress and ~~therefore~~ is quiet. Recurrence time for this earthquake has been estimated to be more than 1,000 years given the regional slow strain rate. However, the eastern normal faults of the system offset the seafloor over more than 30 km and present tilted blocks filled by fan shaped late Pleistocene deposits attesting for recent deformation. In the light of these observations, the eventuality of a tsunamigenic earthquake along these faults should be considered. To the North-West along the Harvers segment, a ~~tsunamigenic~~ rupture occurred in 1985 with ~~strike-slip kinematics and a~~  $M_w$  ~~6.5~~ earthquake showing strike-slip mechanisms. Beck et al., (2012) estimated a recurrence time of 6,500-7,000 years for such a  $M_w$  ~~6.5~~ event based on the vertical offset of coseismic deposits in hemipelagites imaged by very high-resolution seismic lines across the fault. In between these two segments, the Montserrat-Bouillante segment is seismically quiet except if the 1897 (estimated  $M_w$  ~~7.0~~) earthquake occurred along this fault (Feuillet et al., 2011b). However, no tsunami related to such a rupture has been reported. Seismic lines across the Montserrat-Bouillante fault (Feuillet et al., 2010; Legendre, 2018) reveal that the fault offsets the most recent units including the oldest reflector drilled during the IODP1395, that dates upper Gelasian *ca.* 1.8-2Ma (Le Friant et al. 2013). Given an offset of 0.3m ~~stwt~~ and a 2000-2500 m/s sediments velocity this provides a 0.15-0.2 mm·yr<sup>-1</sup> ~~mm·yr<sup>-1</sup>~~ slip rate. Thus, the Montserrat-Bouillante segment should also be considered tsunamigenic (Figure 2).

South of Grande-~~Terre~~ of Guadeloupe, the N90°E trending Gosier Fault system bounds 45 km of coastal area (Figure 2). The fault system offset the Mid-Pleistocene Grande-Terre plateau that culminates at +150 m from the offshore plateau that rests 15-20 mbsl (Münch et al., 2013). This suggests a long-term vertical slip rate *ca.* 0.10 mm·yr<sup>-1</sup> ~~1mm·yr<sup>-1</sup>~~. To the east of Grande-Terre, the fault crosscuts the MIS5e terrace attesting for

719 Late Pleistocene activity of the fault. However, evaluation of paleo-seismicity along one  
720 eastern segment of the fault system by the means of trenches allowed the identification  
721 of recent surface ruptures, although superficial deposits remain undated (Terrier and  
722 Combes, 2002).

723 East of Guadeloupe, offshore, the Marie-Galante Basin is bounded to the east by  
724 the Karukera spur ([Figure 2D](#)), a 75 km long N-S trending submerged plateau that  
725 culminates 30 mbsl to the north offshore La Désirade Island, and gently dips southward  
726 down to *ca.* 1500 mbsl (De Min et al., 2015). The spur is bounded to the west by N150°E  
727 to N0°E trending, west dipping, and normal faults. These faults offset the middle Miocene  
728 sequence boundary (SB2) by up to *ca.* 2,700-2,900 m, leading to a long-term vertical slip  
729 rate of 0.16-0.18 ~~mm·yr<sup>-1</sup>~~<sup>mm·yr<sup>-1</sup></sup>. Recent deposits are clearly affected by tectonic activity  
730 (Siebert et al., 2020). Located far from the islands, the earthquake intensity felt onshore  
731 would be relatively low in the island, but a tsunami could propagate across the Marie-  
732 Galante Basin directly toward the [coasts of the Lesser Antilles](#) ~~a~~ Arc islands ~~coast~~.

733

## 734 5.2. Slip rate reassessment along the Morne Piton ~~f~~Fault system

735

736 ~~With this study, we evidence that the slip rate along the Morne Piton fault system~~  
737 ~~increases through time with a maximum slip rate of 0.25 ±0.08 mm·yr<sup>-1</sup> since the last 1.29~~  
738 ~~Ma. This slip rate is up to four times slower than previous estimates.~~ Over the last 330 Ka,  
739 Feuillet et al. (2004) estimate a bulk slip rate along the Morne Piton ~~f~~Fault as high as 1  
740 ~~mm·yr<sup>-1</sup>~~<sup>mm·yr<sup>-1</sup></sup> over 330 – 125 Ka then decreasing to 0.3 ~~mm·yr<sup>-1</sup>~~<sup>mm·yr<sup>-1</sup></sup> since the last  
741 125 Ka. This ~~latter-last~~ value is close to the long-term slip rate obtained offshore in this  
742 study (Figure 11). These results suggest that the fault may present a fast slip rate during  
743 short periods of time (few 100 ka.) separated by long periods (million years) of low slip  
744 rate. The ~~fast~~ 1 ~~mm·yr<sup>-1</sup>~~<sup>mm·yr<sup>-1</sup></sup> rate was obtained considering that the terrace T2MG is  
745 offset by the fault by 159 m and dates MIS7e (249 Ka) and the upper-plateau of Marie-  
746 Galante corresponds to an abrasion surface from the MIS9e high stand (330 Ka) (Feuillet  
747 et al., 2004).

748 ~~This latter statement can be reconsidered. The same *Agaricia sp.* limestone unit, *Agaricia,*  
749 ~~and *Acropora sp.* limestone unit, top the 3three islands, Grande-Terre – La Désirade –~~  
750 ~~Marie Galante, suggesting they emerged synchronously (Feuillet et al., 2002; Cornée et~~  
751 ~~al., 2012; Munch et al., 2013). In La Désirade, the Upper Plateau culminates at 276 m asl~~~~

752 ~~(above sea level), whereas the 330 Ka terrace is at 35 m asl (Lardeaux et al., 2014; Leticée~~  
753 ~~et al., 2019). Consequently, the hypothesis stating that the plateau emerged 330 Ka ago is~~  
754 ~~ruled out in Marie-Galante as~~ In the 3 islands this the youngest formation, Acropora unit,  
755 ~~of Marie-Galante Plateau~~ is not younger than 1.07 Ma and not older than 1.54Ma (Cornée  
756 et al., 2012; Münch et al., 2014). From the geological map of Bouysse et al. (1993), this  
757 ~~later~~-unit rims Marie-Galante Island. In La Désirade, the Upper Plateau culminates at 276  
758 m asl (above sea level), whereas the 330 Ka terrace is at 35 m asl (Lardeaux et al., 2014;  
759 Leticée et al., 2019). Consequently, the hypothesis stating that the plateau emerged 330  
760 Ka ago can be ruled out in Marie-Galante.  
761 ~~Thus, Considering~~ Based on this formation as the age of the latest deposit ~~at of~~ the Marie-  
762 Galante Plateau that range between 1.54 and 1.07 Ma, it provides a vertical slip rate of  
763 0.15-0.22 ~~mm·yr<sup>-1</sup>~~ mm·yr<sup>-1</sup> can be calculated. This ~~, a~~ value is close to the ca. 0.25 mm·yr<sup>-1</sup>  
764 ~~1mm·yr<sup>-1</sup>~~ obtained offshore for the slip rate along the Morne Piton ~~f~~Fault system over the  
765 same period of time (Figure 11). As a consequence, it is not possible to conclude that the  
766 Morne Piton ~~f~~Fault system has short periods of fast slip rate, but ~~it instead most~~ instead  
767 it probably evolves-increases through time, ~~with a rather constant~~ reaching a maximum  
768 slip rate of 0.25 mm·yr<sup>-1</sup> over the last million years. ~~0.2mm·yr<sup>-1</sup>.~~ ~~As a consequence,~~  
769 Dividing by four the slip rate along the Morne Piton fault system is increasing the  
770 earthquake time recurrence along this fault system and thus the time recurrence of  
771 potential associated tsunami. ~~This slip rate is five times slower than previous estimates~~  
772 ~~along Morne Piton, considerably increasing the earthquake time recurrence along this~~  
773 ~~fault system and thus the time recurrence of potential associated tsunami.~~  
774 Constraining the fault slip rate at the time scale of one or few seismic cycles may allow  
775 better estimates of seismic and tsunamigenic hazards of the Morne Piton ~~f~~Fault system.  
776 This would require a better knowledge of in-depth fault geometry and identification of  
777 its active segments that could be obtained by the means of a microseismic survey (using  
778 Ocean Bottom Seismometers acquisition over 1-2 years or more). At present-day, BOTDR  
779 laser reflectometry is used to perform long-term monitoring of the Morne Piton ~~f~~Fault  
780 using the network of submarine telecom fiber optic cables connecting Marie-Galante to  
781 the larger islands of Basse-Terre and Grande-Terre (Gutscher et al., 2023). It is to note  
782 that given the slow strain rate and in the absence of rupture occurring along the fault  
783 during the survey period, identifying slip rate across this fault system may require ~~one~~  
784 hundreds to few tensthousands of years. Moreover, very high-resolution seismic data



785 across the fault in areas of high sedimentation rates (*i.e.*, along the eastern coast of Basse-  
786 Terre Island) may constrain the Holocene fault activity. Slip rate estimates ~~will~~ can be  
787 obtained by coring and dating ~~of (i) of~~ the most recent deformed sediments ~~as well as (ii)~~  
788 tsunami deposits in salt marshes. Finally, such regional monitoring ~~will~~ would also  
789 contribute to a survey of past and potential landslides that may also be induced by  
790 earthquakes and which may locally generate destructive waves.

### 791 792 5.3. Bathymetric features control on tsunami wave propagation 793 simulation

794 The aim of the tsunami simulation associated to the present study is not to  
795 produce a precise hazard assessment for the islands of Guadeloupe, but rather to give an  
796 overview of what could happen in terms of tsunami generation if ~~the whole~~ all the  
797 identified segments of the Morne Piton ~~f~~ Fault segments system ruptured together, and to  
798 identify a few gaps in terms of scientific knowledge and operational activities. An accurate  
799 hazard assessment study would require many rupture scenarii including combinations  
800 of the segments used in this study, with variations of their parameters and  
801 ~~sensitivity~~ bility tests.

802 The main outcome of the simulation presented ~~herein~~ above lies in the fact that  
803 submarine features play an important role on the tsunami waves behavior and amplitude.  
804 Submarine canyons are ~~{~~ known to focus the waves ~~as: : canyons (e.g.: along the~~  
805 continental slope of the middle American trench: Álvarez-Gómez et al., 2012; or at  
806 Nazarè Portugal: Martins et al., 2010; do Carmo et al., 2022; Delpéy et al., 2021). This  
807 behavior also occurs along the rime of the island submarine plateau rising the wave  
808 amplitude as exemplified in front of the most populated cities of south-eastern Grande-  
809 Terre (Figure 9). ~~and s~~ Shallow water plateaus located around ~~the~~ or between islands  
810 slow down the waves which leads to particular propagation patterns like the wrapping  
811 around the relief islands (Figure 8). ~~In fact, it underlines~~ There, the wrapping effect of the  
812 waves around Marie-Galante and the Colombie Bank results in ~~associated with~~ two  
813 distinct tsunami sources, *i.e.* a primary source at fault and a secondary one at the  
814 Colombie Bank (Figure 8). Such a behavior, already shown in other regions, is able to  
815 considerably amplify the impact of the tsunami on the coast opposite to the fault rupture  
816 (Chadha et al., 2005; Chen et al., 2010). It is important to notice that the low resolution of  
817 the grid used for the present simulations is a limiting factor in quantifying correctly the

818 wave amplitude along the shoreline. A higher resolution simulation grid would better  
819 reproduce the bathymetric features, especially in shallow waters, having a non-negligible  
820 impact on the waves' behavior and amplitude.

821 ~~The Our~~ simulation also highlights interesting phenomena that would require  
822 further consideration in the framework of further tsunami hazard studies: wave  
823 oscillation, which could be attributed to a resonance effect, is clearly visible within the  
824 Les Saintes Archipelago, and potential wave trapping is also visible around those islands.  
825 If the second case is purely observation, the resonance between Les Saintes islands is  
826 clearly revealed by the single-sided Fourier amplitude spectrum (Figure 10) and the peak  
827 at ~~~17.15~~ min seems to be associated with the negative wave coming time after the initial  
828 wave front and related to the tsunami interaction with the Colombie Bank shoal. The  
829 records provided by the virtual gauges located beforehand within the archipelago (VG\_1,  
830 VG\_2 & VG\_3) clearly shows a long-period oscillation of the signal which is not present on  
831 the gauges located outside of Les Saintes (VG\_4, VG\_5, VG\_6 & VG\_11). It shows how the  
832 frequency content of the incoming signal can affect the sea-level during many hours after  
833 the seismic rupture.

834 The numerical simulations ~~performed by Cordrie et al. (2020)~~ of the tsunami  
835 having followed the ~~M<sub>w</sub>M<sub>w</sub>~~ 6.4–3 Les Saintes earthquake were able to match the  
836 witnesses' observations in Les Saintes (~~Cordrie eZahibo et al., 200520~~). Despite the low  
837 resolution (100m) of the present simulation on Les Saintes, there are some similarities  
838 between the two studies of potential impacted zones, for example in Marigot or Grande  
839 Anse Bays. It also shows that other bays, like the ones located between Terre-de-Haut and  
840 Ilet à Cabrit, appear to be quite well protected and not exposed to relatively strong  
841 tsunami waves.

842 Finally, this study also highlights the exposed coastline of Dominica: on the north-  
843 northeast coast of the island (Figure 9), 50+ cm waves are simulated, showing that this  
844 island should integrate such a scenario of crustal fault rupture within its tsunami hazard  
845 assessment plan.

846

## 847 ***Conclusions***

848

849 Thanks to HR bathymetry, reflection seismic data and rock/sediment samples, the  
850 analyses of the morphology and tectonic structures of the Marie Galante Basin located in

851 the middle of the Guadeloupe Archipelago, allow to detail the structural pattern of this  
852 region and to estimate a ~~constant~~ slip rate of *ca.* ~~0.125 mm·yr<sup>-1</sup>~~ mm·yr<sup>-1</sup> increasing over  
853 the last million year to 0.25 mm·yr<sup>-1</sup>, ~~a~~ along the Morne Piton ~~f~~Fault system, ~~cross-cutting~~  
854 the basin, ~~since its inception (i.e. over that last 7 Ma)~~. This estimate divides the previously  
855 published estimations of the slip rate by ~~four~~five, and thus increases the earthquake  
856 recurrence time associated to the Morne Piton ~~f~~Fault system from 1Ka to ~~4-5-6~~ Ka. We  
857 show that a seismic rupture associated to an earthquake showing a moment magnitude  
858 ~~M<sub>w</sub>~~M<sub>w</sub> ~6.5 can occur along the Morne Piton ~~F~~Fault system in case of the rupture of the  
859 full length of the fault (all segments being considered connected at depth in the present  
860 demonstration). Such an event would be tsunamigenic according to numerical simulation  
861 results. The multi-segment tsunami modeling illustrates how submarine morphological  
862 and structural features influences the propagation pattern of the tsunami leading to  
863 constructing interferences and resonances, thus increasing the tsunami threat on nearby  
864 islands, especially highlighting a resonance effect within the Les Saintes Islands, not  
865 discussed so far (and potentially the explanation of the ~~so-far 2004 non-un~~reproduced  
866 run-up values of the 2004 tsunami). At a regional scale we evidenced that several other  
867 regional faults such as Montserrat-Harvers-Bouillante Fault, Gosier Fau~~l~~t, Karukera Spur  
868 ~~border~~Border ~~F~~Fault, may also be tsunamigenic. Indeed, although they have the potential  
869 to produce relatively low magnitude (<7) earthquakes, their rupture could occur at  
870 shallow depth and close to a highly populated coast. Therefore, scenarii with arc and  
871 forearc crustal fault ruptures must be integrated within their tsunami hazard assessment  
872 plan. For that, it is necessary to have a better knowledge of onshore-offshore structural  
873 and seismogenic patterns of each individual major faults system as the regional low strain  
874 rate leads to large recurrence time of tsunamigenic earthquakes (>1,000 years), *i.e.* much  
875 greater than the historical record. In addition, these earthquakes could also have the  
876 capacity to destabilize the sedimentary layers at the edge of plateaus and canyons,  
877 triggering submarine mass failures, capable of triggering large but more localized  
878 tsunamis.

### 879 ***Competing interests***

880 The contact author has declared that none of the authors has any competing interests.  
881  
882  
883

### 884 ***Acknowledgements and data***

885  
886  
887  
888  
889  
890  
891  
892  
893  
894  
895  
896  
897  
898  
899  
900  
901  
902  
903  
904  
905  
906

We are grateful to C. Deplus, A. Hirn (IPGP) and M. Laigle (GeoAzur) for providing Aguadomar and Sismantilles seismic and bathymetry data and to I Thinon and P. Gennoc (BRGM) for providing the Geoberyx seismic Data. The Kashallow project was supported by The French National Program DyETI from INSU-CNRS, by the European Interreg IIB “Caribbean Space” Fund engaged in Guadeloupe with the EFRD projects (op. 30-700) and the Region Guadeloupe. Part of this study was funded by the New Zealand’s Strategic Science Investment Fund (SSIF).

***Data availability and request***

Litto3D data can be found at <https://diffusion.shom.fr/loisir/litto3d-guad2016.html>  
French oceanographic fleet data can be obtain on demand via the Simer online interface following the cruise doi – Aguadomar: <https://doi.org/10.17600/98010120>; Sismantilles: <https://doi.org/10.17600/1080060> and <https://doi.org/10.17600/7010020>; Kashallow: <https://doi.org/10.17600/9020010>;

Requests for the Geoberyx03 data must be addressed to the BRGM.  
Some figures have been prepared using the Generic Mapping Tools Version 6 software (Wessel et al., 2019).

## 907 **References**

- 908
- 909 Accary, F., & Roger, J., 2010. Tsunami catalog and vulnerability of Martinique (Lesser Antilles,  
910 France). *Science of Tsunami Hazards*, 29(3).
- 911 Ajvazi, B., & Czimber, K., 2019. A comparative analysis of different DEM interpolation methods in  
912 GIS: case study of Rahovec, Kosovo. *Geodesy and cartography*, 45(1), 43-48.  
913 <https://doi.org/10.3846/gac.2019.7921>
- 914 Arun, P.V., 2013. A comparative analysis of different DEM interpolation methods. *The Egyptian,*  
915 *Journal of Remote Sensing and Space Science*, 16(2), 133-139.  
916 <https://doi.org/10.1016/j.ejrs.2013.09.001>
- 917 Barkan, R. and Ten Brink, U., 2010. Tsunami simulations of the 1867 virgin island earthquake:  
918 Constraints on epicenter location and fault parameterstsunami simulations of the 1867  
919 virgin island earthquake: Constraints on epicenter location. *Bulletin of the Seismological*  
920 *Society of America*, 100(3), pp.995-1009. <https://doi.org/10.1785/0120090211>
- 921 Bazin, S., Feuillet, N., Duclos, C., Crawford, W., Nercessian, A., Bengoubou-Valerius, M., ... & Singh,  
922 S. C., 2010. The 2004–2005 Les Saintes (French West Indies) seismic aftershock sequence  
923 observed with ocean bottom seismometers. *Tectonophysics*, 489(1-4), 91-103.  
924 <https://doi.org/10.1016/j.tecto.2010.04.005>
- 925 Beck, C., Reyss, J.L., Leclerc, F., Moreno, E., Feuillet, N., Barrier, L., Beauducel, F., Boudon, G.,  
926 Clément, V., Deplus, C. and Gallou, N., 2012. Identification of deep subaqueous co-seismic  
927 scarps through specific coeval sedimentation in Lesser Antilles: implication for seismic  
928 hazard. *Natural Hazards and Earth System Sciences*, 12(5), pp.1755-1767.  
929 <https://doi.org/10.5194/nhess-12-1755-2012>
- 930 Bernard, P., & Lambert, J., 1988. Subduction and seismic hazard in the northern Lesser Antilles:  
931 Revision of the historical seismicity. *Bulletin of the Seismological Society of America*, 78(6),  
932 1965-1983.
- 933
- 934 Bernardes, T., Gontijo, I., Andrade, H., Vieira, T.G.C., Alves, H.M.R., 2006. Digital Terrain Models  
935 Derived from SRTM Data and Kriging. In: AbdulRaman A., Zlatanova S., Coors V. (eds)  
936 Innovations in 3D Geo Information Systems. Lecture Notes in Geoinformation and  
937 Cartography. Springer, Berlin, Heidelberg. [https://doi.org/10.1007/978-3-540-36998-](https://doi.org/10.1007/978-3-540-36998-1_51)  
938 [1\\_51](https://doi.org/10.1007/978-3-540-36998-1_51)
- 939

- 940 Bie, L., Rietbrock, A., Hicks, S., Allen, R., Blundy, J., Clouard, V., Collier, J., Davidson, J., Garth, T.,  
941 Goes, S., Harmon, N., Henstock; T., van Huenen, J., Kendall, M., Krüger, F., Lynch, L.,  
942 Macpherson, C., Robertson, R., Tait, S., Wilknison, J. & Wilson, M., 2020. Along-arc  
943 heterogeneity in local seismicity across the Lesser Antilles subduction zone from a dense  
944 ocean-bottom seismometer network. *Seismological Research Letters*, 91(1), 237-247.  
945 <https://doi.org/10.1785/0220190147>
- 946 Biggs, J., & Wright, T. J., 2020. How satellite InSAR has grown from opportunistic science to  
947 routine monitoring over the last decade. *Nature Communications*, 11(1), 1-  
948 4.<https://doi.org/10.1038/s41467-020-17587-6>
- 949 Bilek, S. L. (2010). Invited review paper: Seismicity along the South American subduction zone:  
950 Review of large earthquakes, tsunamis, and subduction zone complexity. *Tectonophysics*,  
951 495(1-2), 2-14. <https://doi.org/10.1016/j.tecto.2009.02.037>
- 952 Boucard, M., Marcaillou, B., Lebrun, J. F., Laurencin, M., Klingelhoefer, F., Laigle, M., Lallemand, S.,  
953 Schenini, L., Graindorge, D., Cornee, J.J., Münch, P. & Philippon, M., 2021. Paleogene V-  
954 shaped basins and Neogene subsidence of the Northern Lesser Antilles Forearc. *Tectonics*,  
955 40(3), e2020TC006524. <https://doi.org/10.1029/2020TC006524>
- 956 Bouysse P., Garrabé F., Mauboussin T., Andreieff P., Battistini R., Carlier P., Hinschberger F. &  
957 Rodet J. (1993). – Carte géologique du département de la Guadeloupe. Notice explicative:  
958 Marie-Galante et îlets de la Petite-Terre, scale 1: 50, 000. – BRGM, Orléans, France.
- 959 Bouysse, P., Mascle, A. (1994). Sedimentary Basins and Petroleum Plays Around the French  
960 Antilles. In: Mascle, A. (eds) *Hydrocarbon and Petroleum Geology of France*. Special  
961 Publication of the European Association of Petroleum Geoscientists, vol 4. Springer, Berlin,  
962 Heidelberg. [https://doi.org/10.1007/978-3-642-78849-9\\_32](https://doi.org/10.1007/978-3-642-78849-9_32).
- 963 Chadha, R. K., Latha, G., Yeh, H., Peterson, C., & Katada, T. (2005). The tsunami of the great  
964 Sumatra earthquake of M 9.0 on 26 December 2004–Impact on the east coast of India.  
965 *Current Science*, 1297-1301.
- 966 Chen, J. M., Liang, D., & Tang, H. (2012). Interaction between tsunami waves and isolated conical  
967 islands. *Journal of Coastal Research*, 28(5), 1270-1278.
- 968 Colon Useche, S., Clouard, V., Ioualalen, M., Audemard, F. and Monfret, T., 2023. Simulation of  
969 tsunami inundation for the island of Martinique to nearby large earthquakes. *Bulletin of the*

970 *Seismological Society of America*, 113(1), pp.252-267.  
 971 <https://doi.org/10.1785/0120220093>

972 Corbeau, J., Feuillet, N., Lejeune, A. M., Fontaine, F. R., Clouard, V., Saurel, J. M., & OVSM team, 2021.  
 973 A significant increase in interplate seismicity near major historical earthquakes offshore  
 974 martinique (FWI). *Bulletin of the Seismological Society of America*, 111(6), 3118-3135.  
 975 <https://doi.org/10.1785/0120200377>

976 Cordrie, L., Gailler, A., Escartin, J., Feuillet, N., & Heinrich, P., 2020. Simulation of the 2004 tsunami  
 977 of Les Saintes in Guadeloupe (Lesser Antilles) using new source constraints. *Natural*  
 978 *Hazards*, 103(2), 2103-2129. <https://doi.org/10.1007/s11069-020-04073-x>

979 Cornée, J. J., Leticée, J. L., Münch, P., Quillevere, F., Lebrun, J. F., Moissette, P., Braga, C., Melinte-  
 980 Dobrinescu, M., De Min, L., Oudet, J. & Randrianasolo, A., 2012. Sedimentology,  
 981 palaeoenvironments and biostratigraphy of the Pliocene–Pleistocene carbonate platform  
 982 of Grande-Terre (Guadeloupe, Lesser Antilles forearc). *Sedimentology*, 59(5), 1426-1451.  
 983 <https://doi.org/10.1111/j.1365-3091.2011.01311.x>

984 Cornée, J. J., Münch, P., Philippon, M., Boudagher-Fadel, M., Quillévéré, F., Melinte-Dobrinescu, M.,  
 985 Lebrun, J.F., Meyer, S., Montheil, L., Lallemand, S., Marcaillou, B., Laurencin, M., Legndre, L.,  
 986 Garrocq, C., Boucard, M., Beslier, M.O., Laigle, M., Schenini, L., Fabre, P.H. & Marivaux, L.,  
 987 2021. Lost islands in the northern Lesser Antilles: possible milestones in the Cenozoic  
 988 dispersal of terrestrial organisms between South-America and the Greater Antilles. *Earth-*  
 989 *Science Reviews*, 217, 103617. <https://doi.org/10.1016/j.earscirev.2021.103617>

990 Cornée, J.J., De Min, L., Lebrun, J.F., Quillévéré, F., Melinte-Dobrinescu, M., BouDagher-Fadel, M.,  
 991 Montheil, L. , Marcaillou, B., Thinon, I. and Philippon M., 2023. Paleogeographic evolution  
 992 and vertical motion of the central Lesser Antilles forearc since the Early Miocene: A  
 993 potential driver for land fauna dispersals between the americas. *Marine and Petroleum*  
 994 *Geology*, 152, 106264. <https://doi.org/10.1016/j.marpetgeo.2023.106264>

995 Dao, M. H., & Tkalich, P., 2007. Tsunami propagation modelling—a sensitivity study. *Natural*  
 996 *Hazards and Earth System Sciences*, 7(6), 741-754. [https://doi.org/10.5194/nhess-7-741-](https://doi.org/10.5194/nhess-7-741-2007)  
 997 [2007](https://doi.org/10.5194/nhess-7-741-2007)

998 Delpéy, M., Lastiri, X., Abadie, S., Roeber, V., Maron, P., Liria, P., & Mader, J. (2021).  
 999 Characterization of the wave resource variability in the French Basque coastal area based  
 1000 on a high-resolution hindcast. *Renewable Energy*, 178, 79-95.  
 1001 <https://doi.org/10.1016/j.renene.2021.05.167>

1002 DeMets, C., Jansma, P. E., Mattioli, G. S., Dixon, T. H., Farina, F., Bilham, R., Calais, E. & Mann, P.,  
1003 2000. GPS geodetic constraints on Caribbean-North America plate motion. *Geophysical*  
1004 *Research Letters*, 27(3), 437-440. <https://doi.org/10.1029/1999GL005436>

1005 De Min, L., 2014. Sismo-stratigraphie multi-échelles d'un bassin d'avant-arc: le bassin de Marie-  
1006 Galante, Petites Antilles (Doctoral dissertation, Antilles-Guyane).

1007 De Min, L., Lebrun, J. F., Cornée, J. J., Münch, P., Léticée, J. L., Quillévéré, F., Melinte-Dobrinescu, M.,  
1008 Randrianasolo, A., Marcaillou, B. & Zami, F., 2015. Tectonic and sedimentary architecture of  
1009 the Karukéra spur: A record of the Lesser Antilles fore-arc deformations since the Neogene.  
1010 *Marine Geology*, 363, 15-37. <https://doi.org/10.1016/j.margeo.2015.02.007>

1011 Deplus C., 1998, AGUADOMAR cruise, RV L'Atalante, <https://doi.org/10.17600/98010120>

1012 Dix, C.H., 1955. Seismic Velocities from Surface Measurements," *Geophysics* 20, no. 1, 68-86.  
1013 <https://doi.org/10.1190/1.1438126>

1014 [Deplus, C., Le Friant, A., Boudon, G., Komorowski, J.C., Villemant, B., Harford, C., Ségoufin, J. and Cheminée,](#)  
1015 [J.L., 2001. Submarine evidence for large-scale debris avalanches in the Lesser Antilles Arc. \*Earth\*](#)  
1016 [and Planetary Science Letters, 192\(2\), pp.145-157.](#)

1017 do Carmo, J. S. A. (2022). Dominant processes that amplify the swell towards the coast: the  
1018 Nazaré Canyon and the giant waves. *Research, Society and Development*, 11(11),  
1019 e578111133804-e578111133804. <https://doi.org/10.33448/rsd-v11i11.33804>

1020 Escartín, J., Leclerc, F., Olive, J. A., Mevel, C., Cannat, M., Petersen, S., Augustin, N., Feuillet, N.,  
1021 Deplus, C., Bezos, A., Bonnemains, D., Chavagnac, V., Choi, Y., Godard, M., Haaga, K., Hamelin,  
1022 C., Ildefonse, B., Jamieson, J.W., John, B.E., Leleu, T., MacLead, C.J., Massot-Campos, M.,  
1023 Nomikou, P., Paquet, M., Tominaga, M., Triebe, L., Campos, R., Gracias, N., Garcia, R.,  
1024 Andreani, M. & Vilaseca, G. (2016). First direct observation of coseismic slip and seafloor  
1025 rupture along a submarine normal fault and implications for fault slip history. *Earth and*  
1026 *Planetary Science Letters*, 450, 96-107. <https://doi.org/10.1016/j.epsl.2016.06.024>

1027 Escartin, J., Leclerc, F., Nathalie, F., Le Friant, A., Billant, J., Olive, J. A. L., Henri, M., Andreani, M.,  
1028 Arnaubec, A., Dano, A., Delorme, A., Deplus, C., Fournasson, M.L., Gini, C., Gracias, N.,  
1029 Hamelin, C., Istenic, K., Komorowski, J.C., Marchand C., Mevel, C., Onstad, S., Quidelleur, X. &  
1030 Garcia, R. (2018, December). Mapping the  $M_w$ - $M_w$  6.3 2004 Les Saintes earthquake seafloor  
1031 rupture with deep-sea vehicles: Length, displacement, nature, and links between coseismic  
1032 deformation and erosion/sedimentation. In *AGU Fall Meeting Abstracts* (Vol. 2018, pp.  
1033 EP51D-1851).



- Feuillet, N., 2000. Sismotectonique des Petites Antilles: Liaison entre activité sismique et volcanique (Doctoral dissertation, Paris 7).
- 1034 Feuillet, N., Manighetti, I., & Tapponnier, P., 2001. Extension active perpendiculaire à la  
1035 subduction dans l'arc des Petites Antilles (Guadeloupe, Antilles françaises). Comptes  
1036 Rendus de l'Académie des Sciences-Series IIA-Earth and Planetary Science, 333(9), 583-  
1037 590.
- 1038 Feuillet, N., Manighetti, I., Tapponnier, P., & Jacques, E., 2002. Arc parallel extension and  
1039 localization of volcanic complexes in Guadeloupe, Lesser Antilles. Journal of Geophysical  
1040 Research: Solid Earth, 107(B12), ETG-3. <https://doi.org/10.1029/2001JB000308>
- 1041 Feuillet, N., Tapponnier, P., Manighetti, I., Villemant, B., & King, G. C. P., 2004. Differential uplift  
1042 and tilt of Pleistocene reef platforms and Quaternary slip rate on the Morne-Piton normal  
1043 fault (Guadeloupe, French West Indies). Journal of Geophysical Research: Solid Earth,  
1044 109(B2). <https://doi.org/10.1029/2003JB002496>
- 1045 Feuillet, N., Leclerc, F., Tapponnier, P., Beauducel, F., Boudon, G., Le Friant, A., Deplus, C., Lebrun,  
1046 J.F., Necessian, A., Saurel, J.M. & Clément, V., 2010. Active faulting induced by slip  
1047 partitioning in Montserrat and link with volcanic activity: New insights from the 2009  
1048 GWADASEIS marine cruise data. Geophysical Research Letters, 37(19).  
1049 <https://doi.org/10.1029/2010GL042556>
- 1050 Feuillet, N., Beauducel, F., & Tapponnier, P., 2011. Tectonic context of moderate to large historical  
1051 earthquakes in the Lesser Antilles and mechanical coupling with volcanoes. Journal of  
1052 Geophysical Research: Solid Earth, 116(B10). <https://doi.org/10.1029/2011JB008443>
- 1053 Fujita, M., Ishikawa, T., Mochizuki, M., Sato, M., Toyama, S. I., Katayama, M., Kawai, K., Mastumoto,  
1054 Y., Yabuki, T., Asada, A. & Colombo, O. L., 2006. GPS/Acoustic seafloor geodetic observation:  
1055 method of data analysis and its application. Earth, planets and space, 58(3), 265-275.  
1056 <https://doi.org/10.1186/BF03351923>
- 1057 GEBCO Compilation Group, 2021. GEBCO 2021 Grid (doi:10.5285/c6612cbe-50b3-0cff-e053-  
1058 6c86abc09f8f)
- 1059 Geli, L., Çağatay, N., Gasperini, L., Favali, P., Henry, P., & Çifçi, G., 2011. ESONET WP4-  
1060 Demonstration Missions. MARMARA-DM final report.  
1061 <https://archimer.ifremer.fr/doc/00032/14324/>
- 1062 Goldfinger, C., Nelson, C. H., Morey, A. E., Johnson, J. E., Patton, J. R., Karabanov, E. B., Gutierrez-  
1063 Pastor, J., Eriksson, A.T., Gracia, E., Dunhill, G., Enkin, R.J., Dallimore, A. & Vallier, T., 2012.  
1064 Turbidite event history—Methods and implications for Holocene paleoseismicity of the

1065 Cascadia subduction zone(No. 1661-F). US Geological Survey.  
1066 <https://doi.org/10.3133/pp1661F>

1067 Gonzalez, OL, Clouard, V., & Zahradnik, J., 2017. Moment tensor solutions along the central Lesser  
1068 Antilles using regional broadband stations. *Tectonophysics*, 717, 214-225.  
1069 <https://doi.org/10.1016/j.tecto.2017.06.024>

1070 Gusman, A.R., Supendi, P., Nugraha, A.D., Power, W., Latief, H., Sunendar, H., Widiyantoro, S.,  
1071 Daryono, Wiyono, S.H., Hakim, A., Muhari, A., Wang, X., Burbidge, D., Palgunadi, K., Hamling,  
1072 I., Daryono, M.R., 2019. Source model for the tsunami inside Palu Bay following the 2018  
1073 Palu earthquake, Indonesia. *Geophysical Research Letters*, 46, 8721-8730,  
1074 <https://doi.org/10.1029/2019GL082717>.

1075 Gusman, A.R., Roger, J., Power, W., Fry, B., Kaneko, Y., 2022. The 2021 Loyalty Islands earthquake  
1076 (~~M<sub>w</sub>~~M<sub>w</sub>7.7): Tsunami waveform inversion and implications for tsunami forecasting for  
1077 New Zealand. *Earth and Space Science*, e2022EA002346,  
1078 <https://doi.org/10.1029/2022EA002346>.

1079 Gutscher, M. A., Royer, J. Y., Graindorge, D., Murphy, S., Klingelhoefer, F., Aiken, C., Cattaneo, A.,  
1080 Barreca, G., Quetel, L., Riccobene, G., Petersen, F., Urlaub, M., Krastel, S., Gross, F., Kopp, H.,  
1081 Margheriti, L. Beranzoli, L., 2019. Fiber optic monitoring of active faults at the seafloor: I  
1082 the FOCUS project. *Photonics*, 32-37. <https://doi.org/10.1051/photon/2019S432>

1083 Hirata, K., Aoyagi, M., Mikada, H., Kawaguchi, K., Kaiho, Y., Iwase, R., Morita, S., Fujisawa, I.,  
1084 Sugioka, H., Mitsuzawa, K., Suyehiro, K. & Fujiwara, N., 2002. Real-time geophysical  
1085 measurements on the deep seafloor using submarine cable in the southern Kurile  
1086 subduction zone. *IEEE Journal of Oceanic Engineering*, 27(2), 170-181.  
1087 <https://doi.org/10.1109/JOE.2002.1002471>

1088 IOC-UNESCO (2020). Experts Meeting on Sources of Tsunamis in the Lesser Antilles Fort-de-  
1089 France, Martinique (France) 18–20 March 2019. Workshop Reports, (291), 55p. Open  
1090 Access version : <https://archimer.ifremer.fr/doc/00665/77736/>

1091 Kido, M., Fujimoto, H., Miura, S., Osada, Y., Tsuka, K., & Tabei, T., 2006. Seafloor displacement at  
1092 Kumano-nada caused by the 2004 off Kii Peninsula earthquakes, detected through repeated  
1093 GPS/Acoustic surveys. *Earth, planets and space*, 58(7), 911-915.  
1094 <https://doi.org/10.1186/BF03351996>

1095 Kopp, H., Weinzierl, W., Becel, A., Charvis, P., Evain, M., Flueh, E. R., Gailler, A., Galve, A., Hirn, A.,  
1096 Kandilarov, D., Klaeschen, D., Laigle, M., Papenberg, C., Planert, L. & Roux, E., 2011. Deep  
1097 structure of the central Lesser Antilles Island Arc: relevance for the formation of

1098 continental crust. *Earth and Planetary Science Letters*, 304(1-2), 121-134.  
1099 <https://doi.org/10.1016/j.epsl.2011.01.024>

1100 Laigle M., Lebrun J.-F., Hirn A. (2007) SISMANTILLES 2 cruise, RV L'Atalante,  
1101 <https://doi.org/10.17600/7010020>

1102 Lander, J. F., & Whiteside, L. S., 1997. Caribbean tsunamis: an initial history. In *Caribbean*  
1103 *Tsunami Workshop*, June (pp. 11-13).

1104 Lander, J. F., Whiteside, L. S., & Lockridge, P. A., 2003. Two decades of global tsunamis. *Science of*  
1105 *Tsunami Hazards*, 21(1), 3.

1106 Lardeaux, J. M., Münch, P., Corsini, M., Cornée, J. J., Verati, C., Lebrun, J. F., Guillevere, F., Melinte-  
1107 Dobrinescu, M., Leticee, J.L., Fietzke, J., Mazabraud, Y., Cordrey, F. & Randrianasolo, A., 2013.  
1108 La Désirade island (Guadeloupe, French West Indies): a key target for deciphering the role  
1109 of reactivated tectonic structures in Lesser Antilles arc building. *Bulletin de la Société*  
1110 *géologique de France*, 184(1-2), 21-34. <https://doi.org/10.2113/gssgfbull.184.1-2.21>

1111 Laurencin, M., Graindorge, D., Klingelhofer, F., Marcaillou, B., & Evain, M., 2018. Influence of  
1112 increasing convergence obliquity and shallow slab geometry onto tectonic deformation and  
1113 seismogenic behavior along the Northern Lesser Antilles zone. *Earth and Planetary Science*  
1114 *Letters*, 492, 59-72. <https://doi.org/10.1029/2019GL083490>

1115 Lebrun, J.-F., Cornée, J.-J., Münch, P., Guennoc, P., Thinon, I., Begot, J., Mazabraud, Y., Fournier, F.,  
1116 Feuillet, N., Randrianasolo, A., 2008. La Mission KaShallow 1 - N/O Antéa - 26 avril - 05 Mai  
1117 - Sismique réflexion haute résolution dans le bassin de Marie-Galante - Avant-arc des  
1118 Petites Antilles. Rapport de l'Université des Antilles et de la Guyane.

1119 Leclerc, F., Feuillet, N., & Deplus, C., 2016. Interactions between active faulting, volcanism, and  
1120 sedimentary processes at an island arc: Insights from Les Saintes channel, Lesser Antilles  
1121 arc. *Geochemistry, Geophysics, Geosystems*, 17(7), 2781-2802.  
1122 <https://doi.org/10.1002/2016GC006337>

1123 Le Friant, A., Heinrich, P., & Boudon, G., 2008. Field survey and numerical simulation of the 21  
1124 November 2004 tsunami at Les Saintes (Lesser Antilles). *Geophysical Research Letters*,  
1125 35(12). <https://doi.org/10.1029/2008GL034051>

1126 [Le Friant, A., Boudon, G., Arnulf, A., & Robertson, R. E. \(2009\). Debris avalanche deposits offshore St.](#)  
1127 [Vincent \(West Indies\): impact of flank-collapse events on the morphological evolution of the island.](#)  
1128 [Journal of Volcanology and Geothermal Research, 179\(1-2\), 1-10.](#)

1129 [Le Friant, A., Lebas, E., Brunet, M., Lafuerza, S., Hornbach, M., Coussens, M., Watt, S., Cassidy, M., Talling,](#)  
1130 [P.J. and IODP 340 Expedition Science Party \(2019\). Submarine landslides around volcanic islands:](#)

1131 [A review of what can be learned from the Lesser Antilles Arc. Submarine Landslides: Subaqueous](#)  
1132 [Mass Transport Deposits from Outcrops to Seismic Profiles, pp.277-297.](#)  
1133

1134 Legendre, L., Philippon, M., Münch, P., Leticee, J. L., Noury, M., Maincent, G., Cornee, J.J., Caravati,  
1135 A., Lebrun, J.F. & Mazabraud, Y., 2018. Trench bending initiation: Upper plate strain pattern  
1136 and volcanism. insights from the Lesser Antilles arc, St. Barthelemy island, French West  
1137 Indies. *Tectonics*, 37(9), 2777-2797.

1138 Lehu, R., Lallemand, S., Ratzov, G., Babonneau, N., Hsu, S. K., Lin, A. T., & Dezileau, L., 2016. An  
1139 attempt to reconstruct 2700 years of seismicity using deep-sea turbidites offshore eastern  
1140 Taiwan. *Tectonophysics*, 692, 309-324. <https://doi.org/10.1016/j.tecto.2016.04.030>

1141 Leticee, J. L., Cornee, J. J., Münch, P., Fietzke, J., Philippon, M., Lebrun, J. F., De Min, L., &  
1142 Randrianasolo, A., 2019. Decreasing uplift rates and Pleistocene marine terraces settlement  
1143 in the central lesser Antilles fore-arc (La Désirade Island, 16° N). *Quaternary International*,  
1144 508, 43-59. <https://doi.org/10.1016/j.quaint.2018.10.030>  
1145

1146 [Leslie, S. C., & Mann, P. \(2016\). Giant submarine landslides on the Colombian margin and tsunami risk in](#)  
1147 [the Caribbean Sea. \*Earth and Planetary Science Letters\*, 449, 382-394.](#)

1148 Lewis, K. B. (1980). Quaternary sedimentation on the Hikurangi oblique-subduction and  
1149 transform margin, New Zealand. *Sedimentation in oblique-slip mobile zones*, 171-189.  
1150 <https://doi.org/10.1002/9781444303735.ch10>

1151 Liu, P.L.F., Woo, S.B., Cho, Y.S., 1998. Computer programs for tsunami propagation and  
1152 inundation. Ithaca (NY): Cornell University. Technical Report.

1153 Mallet, R., 1853. Catalogue of Recorded Earthquakes from 1606 B.C. to A.D. 1850, Part I, 1606  
1154 B.C. to 1755 A.D. Report of the 22nd Meeting of the British Association for the Advancement  
1155 of Science, held in Belfast, Sept. 1852, John Murray, London, 177 pp.

1156 Mallet R. (1854). Catalogue of Recorded Earthquakes from 1606 B.C. to A.D. 1850, Part II, 1755  
1157 A.D. to 1784 A.D., Report of the 23rd meeting of the British Association for the  
1158 Advancement of Science, held in Hull, Sept. 1853, John Murray, London, 118-212.

1159 Mallet R. (1855). Catalogue of Recorded Earthquakes from 1606 B.C. to A.D. 1850, Part III, 1784  
1160 A.D. to 1842 A.D., Report of the 24th Meeting of the British Association for the Advancement  
1161 of Science, John Murray, London, 326 pp.

- 1162 Martins, I., Vitorino, J., & Almeida, S. (2010, May). The Nazare Canyon observatory (W Portugal)  
1163 real-time monitoring of a large submarine canyon. In *OCEANS'10 IEEE SYDNEY* (pp. 1-7).  
1164 IEEE.
- 1165 Martínez-Loriente, S., Sallarès, V., & Gràcia, E., 2021. The Horseshoe Abyssal plain Thrust could  
1166 be the source of the 1755 Lisbon earthquake and tsunami. *Communications earth &*  
1167 *environment*, 2(1), 145. <https://doi.org/10.1038/s43247-021-00216-5>
- 1168
- 1169 Massin, F., Clouard, V., Vorobieva, I., Beauducel, F., Saurel, J. M., Satriano, C., Bouin, M. P., & Bertil,  
1170 D. (2021). Automatic picking and probabilistic location for earthquake assessment in the  
1171 lesser antilles subduction zone (1972-2012). In *Comptes Rendus - Geoscience* (Vol. 353,  
1172 Issue S1). Academie des sciences. <https://doi.org/10.5802/crgeos.81>.  
1173 <https://doi.org/10.5802/crgeos.81>
- 1174 McCalpin, J.P. 1996. (Ed.), *Paleoseismology*, Academic Press, London, p. 583
- 1175 Münch, P., Lebrun, J. F., Cornée, J. J., Thinon, I., Guennoc, P., Marcaillou, B. J., Begot, J., Bertrand, G.,  
1176 Bes De Berc, S., Biscarrat, K., Claud, C., De Min, L., Fournier, F., Gailler, L., Grandorge, D.,  
1177 Leticee, J.L., Marie, L., Mazabraud, Y., Melinte-Dobrinescu, M., Moissette, P., Quilevere, F.,  
1178 Verati, C. & Randrianasolo, A., 2013. Pliocene to Pleistocene carbonate systems of the  
1179 Guadeloupe archipelago, French Lesser Antilles: a land and sea study (the KaShallow  
1180 project). *Bulletin de la Société géologique de France*, 184(1-2), 99-110.  
1181 <https://doi.org/10.2113/gssgfbull.184.1-2.99>
- 1182 Münch, P., Cornee, J. J., Lebrun, J. F., Quillevere, F., Verati, C., Melinte-Dobrinescu, M., Demory, B.,  
1183 Smith, F., Jourdan, J.M., Lardeaux, J.M., De Min, L., Leticee, J.L. & Randrianasolo, A., 2014.  
1184 Pliocene to Pleistocene vertical movements in the forearc of the Lesser Antilles subduction:  
1185 insights from chronostratigraphy of shallow-water carbonate platforms (Guadeloupe  
1186 archipelago). *Journal of the Geological Society*, 171(3), 329-341.  
1187 <https://doi.org/10.1144/jgs2013-005>
- 1188 NASA Shuttle Radar Topography Mission (SRTM)(2013). Shuttle Radar Topography Mission  
1189 (SRTM) Global. Distributed by OpenTopography. <https://doi.org/10.5069/G9445JDF>.  
1190 Accessed: 2022-12-07.
- 1191 Nikolkina, I., Zahibo, N., & Pelinovsky, E., 2010. Tsunami in Guadeloupe (Caribbean Sea). *The*  
1192 *Open Oceanography Journal*, 4(1). <https://doi.org/10.2174/1874252101004010044>

1193 Okada, Y., 1985. Surface deformation due to shear and tensile faults in a half-space. Bulletin of  
1194 the seismological society of America, 75(4), 1135-1154.  
1195 <https://doi.org/10.1785/BSSA0750041135>

1196 O'loughlin, K. F., & Lander, J. F., 2003. Caribbean tsunamis: a 500-year history from 1498-1998  
1197 (Vol. 20). Springer Science & Business Media.

1198 Padron, C., Klingelhoefer, F., Marcaillou, B., Lebrun, J. F., Lallemand, S., Garroq, C., Laigle, M.,  
1199 Roest, W.R., Beslier, M.O., Schenini, L., Graindorge, D., Gay, A., Audemard, F., Munch., P. &  
1200 GARANTI Cruise Team., 2021. Deep structure of the Grenada Basin from wide-angle  
1201 seismic, bathymetric and gravity data. Journal of Geophysical Research: Solid Earth, 126(2),  
1202 e2020JB020472. <https://doi.org/10.1029/2020JB020472>

1203 Paris, R., Sabatier, P., Biguenet, M., Bougouin, A., André, G., Roger, J., 2021. A tsunami deposit at  
1204 Anse Meunier, Martinique Island: evidence of the 1755 CE Lisbon tsunami and implication  
1205 for hazard assessment. Marine Geology, 439, 106561,  
1206 <https://doi.org/10.1016/j.margeo.2021.106561>.

1207 Petersen, F., Kopp, H., Lange, D., Hannemann, K., & Urlaub, M., 2019. Measuring tectonic seafloor  
1208 deformation and strain-build up with acoustic direct-path ranging. Journal of Geodynamics,  
1209 124, 14-24. <https://doi.org/10.1016/j.jog.2019.01.002>

1210 Philippon, M., & Corti, G., 2016. Obliquity along plate boundaries. Tectonophysics, 693, 171-182.  
1211 <https://doi.org/10.1016/j.tecto.2016.05.033>

1212 Prasetya, G., Beavan, J., Wang, X., Reyners, M., Power, W., Wilson, K., Lukovic, B., 2011. Evaluation  
1213 of the 15 July 2009 Fjorland, New Zealand tsunami in the source region. Pure and Applied  
1214 Geophysics, 168, 1973-1987, <https://doi.org/10.1007/s00024-011-0282-6>.

1215 Roger, J., Allgeyer, S., Hébert, H., Baptista, M. A., Loevenbruck, A., & Schindelé, F., 2010. The 1755  
1216 Lisbon tsunami in Guadeloupe Archipelago: source sensitivity and investigation of  
1217 resonance effects. The Open Oceanography Journal, 4(1).  
1218 <https://doi.org/10.2174/1874252101004010058>

1219 Roger, J., Baptista, M. A., Sahal, A., Accary, F., Allgeyer, S., & Hébert, H., 2011. The transoceanic  
1220 1755 Lisbon tsunami in Martinique. Pure and Applied Geophysics, 168(6), 1015-1031.  
1221 <https://doi.org/10.1007/s00024-010-0216-8>

1222 Roger, J., Dudon, B., & Zahibo, N., 2013. Tsunami hazard assessment of Guadeloupe Island (FWI)  
1223 related to a megathrust rupture on the Lesser Antilles subduction interface. Natural  
1224 Hazards and Earth System Sciences, 13(5), 1169-1183. [https://doi.org/10.5194/nhess-13-](https://doi.org/10.5194/nhess-13-1169-2013)  
1225 1169-2013

- 1226 Roger, J., Pelletier, B., & Aucan, J. (2019). Update of the tsunami catalogue of New Caledonia using  
1227 a decision table based on seismic data and marigraphic records. *Natural Hazards and Earth*  
1228 *System Sciences*, 19(7), 1471-1483. <https://doi.org/10.5194/nhess-19-1471-2019>
- 1229 Roger, J., Pelletier, B., Gusman, A., Power, W., Wang, X., Burbidge, D., & Duphil, M., 2023. Potential  
1230 tsunami hazard of the southern Vanuatu Subduction Zone: tectonics, case study of the  
1231 Matthew Island tsunami of 10 February 2021 and implication in regional hazard  
1232 assessment. *Natural Hazards and Earth System Sciences*, 23(2), 393-414,  
1233 <https://doi.org/10.5194/nhess-23-393-2023>.
- 1234 [Roger, J.H., Bull, S., Watson, S.J., Mueller, C., Hillman, J.I., Wolter, A., Lamarche, G., Power, W., Lane,](#)  
1235 [E., Woelz, S. and Davidson, S. \(2024\). A review of approaches for submarine landslide-](#)  
1236 [tsunami hazard identification and assessment. \*Marine and Petroleum Geology\*,](#)  
1237 [p.162\(106729\). <https://doi.org/10.1016/j.marpetgeo.2024.106729>.](#)
- 1238 Ruiz, M., Galve, A., Monfret, T., Sapin, M., Charvis, P., Laigle, M., Evain, M., Hirn, A., Flueh, E., Gallart,  
1239 K., Diaz, J., Lebrun, J.F. & Lebrun, J. F., 2013. Seismic activity offshore Martinique and  
1240 Dominica islands (Central Lesser Antilles subduction zone) from temporary onshore and  
1241 offshore seismic networks. *Tectonophysics*, 603, 68-78.  
1242 <https://doi.org/10.1016/j.tecto.2011.08.006>
- 1243 Salichon, J., Lemoine, A., Aochi, H., 2009. Validation of teleseismic inversion of the 2004 ~~M<sub>w</sub>~~  
1244 6.3 Les Saintes, Lesser Antilles, earthquake by 3D finite-difference forward modelling. *Bull.*  
1245 *Seismol. Soc. Am.* 99, 3390–3401. <https://doi.org/10.1785/0120080315>
- 1246 Satake, K., & Tanioka, Y., 1999. Sources of tsunami and tsunamigenic earthquakes in subduction  
1247 zones. *Pure and Applied Geophysics*, 154(3), 467-483.  
1248 <https://doi.org/10.1785/0120120306>
- 1249 Seibert, C., Feuillet, N., Ratzov, G., Beck, C., & Cattaneo, A., 2020. Seafloor morphology and  
1250 sediment transfer in the mixed carbonate-siliciclastic environment of the Lesser Antilles  
1251 forearc along Barbuda to St. Lucia. *Marine Geology*, 428, 106242.  
1252 <https://doi.org/10.1016/j.margeo.2020.106242>
- 1253 [Smith, M. S., & Shepherd, J. B. \(1996\). Tsunami waves generated by volcanic landslides: an assessment of](#)  
1254 [the hazard associated with Kick'em Jenny. \*Geological Society, London, Special Publications\*, 110\(1\),](#)  
1255 [115-123.](#)
- 1256 Symithe, S. J., Calais, E., Haase, J. S., Freed, A. M., & Douilly, R., 2013. Coseismic slip distribution of  
1257 the 2010 M 7.0 Haiti earthquake and resulting stress changes on regional faults. *Bulletin of*

1258 *the Seismological Society of America*, 103(4), 2326-2343.  
1259 <https://doi.org/10.1785/0120120306>

1260 ten Brink, U., Danforth, W., Polloni, C., Andrews, B., Llanes, P., Smith, S., Parker, E., and Uozumi, T.  
1261 2004. New seafloor map of the Puerto Rico trench helps assess earthquake and tsunami  
1262 hazards. *Eos, Transactions American Geophysical Union* 85: 349-360.  
1263 doi:10.1029/2004EO370001.

1264 Terrier, M., Combes P. avec la collaboration de D. Carbon, B. Grellet, O. Sedan (2002) - FAILLES  
1265 ACTIVES ET EVALUATION DE L’ALEA SISMIQUE : Prise en compte des failles actives dans  
1266 l’aménagement du territoire aux Antilles (Martinique et Guadeloupe). Partie 1 :  
1267 Identification des systèmes de failles actives dans l’archipel de la Guadeloupe et l’île de la  
1268 Martinique. Rapport BRGM/RP-51258-FR. 118 pages. 30 figures. 8 tableaux. 4 annexes

1269 [Teeuw, R., Rust, D., Solana, C., Dewdney, C., & Robertson, R. \(2009\). Large coastal landslides and tsunami](#)  
1270 [hazard in the Caribbean. \*Eos, Transactions American Geophysical Union\*, 90\(10\), 81-82.](#)

1271 Thingbaijam, K.K.S., Mai, P.M. and Goda, K., 2017. New Empirical Earthquake Source-Scaling  
1272 Laws ~~New Empirical Earthquake Source-Scaling Laws~~. *Bulletin of the Seismological Society*  
1273 *of America*, 107(5), pp.2225-2246. <https://doi.org/10.1785/0120170017>

1274 Thinon, I, Bitri, A., 2003. GEOBERYX03 cruise, RV Beryx, [Catalogue des campagnes à la mer](#)  
1275 [\(flotteoceanographique.fr\)](#) ;browsed on-line on Seadatanet webportal  
1276 (SISM\_BGM\_FI352003000010, <https://cdi.seadatanet.org/>);

1277 Thinon I., Bitri A., Guennoc P. & Truffert C. (2004). – Levés sismique et magnétique du plateau  
1278 occidental de l’île de Basse-Terre, Guadeloupe (Campagne Geoberyx03). Apports à la  
1279 compréhension du contexte structural du champ géothermique de Bouillante. – BRGM/RP-  
1280 53152-FR, 77.

1281 Thinon, I., Guennoc, P., Bitri, A., Truffert C., 2010, Study of the Bouillante Bay (West Basse-Terre  
1282 Island shelf): contribution of geophysical surveys to the understanding of the structural  
1283 context of Guadeloupe (French West Indies - Lesser Antilles). *Bull. Soc. Geol. Fr.*, 181, 51-  
1284 65, <http://doi.org/10.2113/gssgfbull.181.1.51>

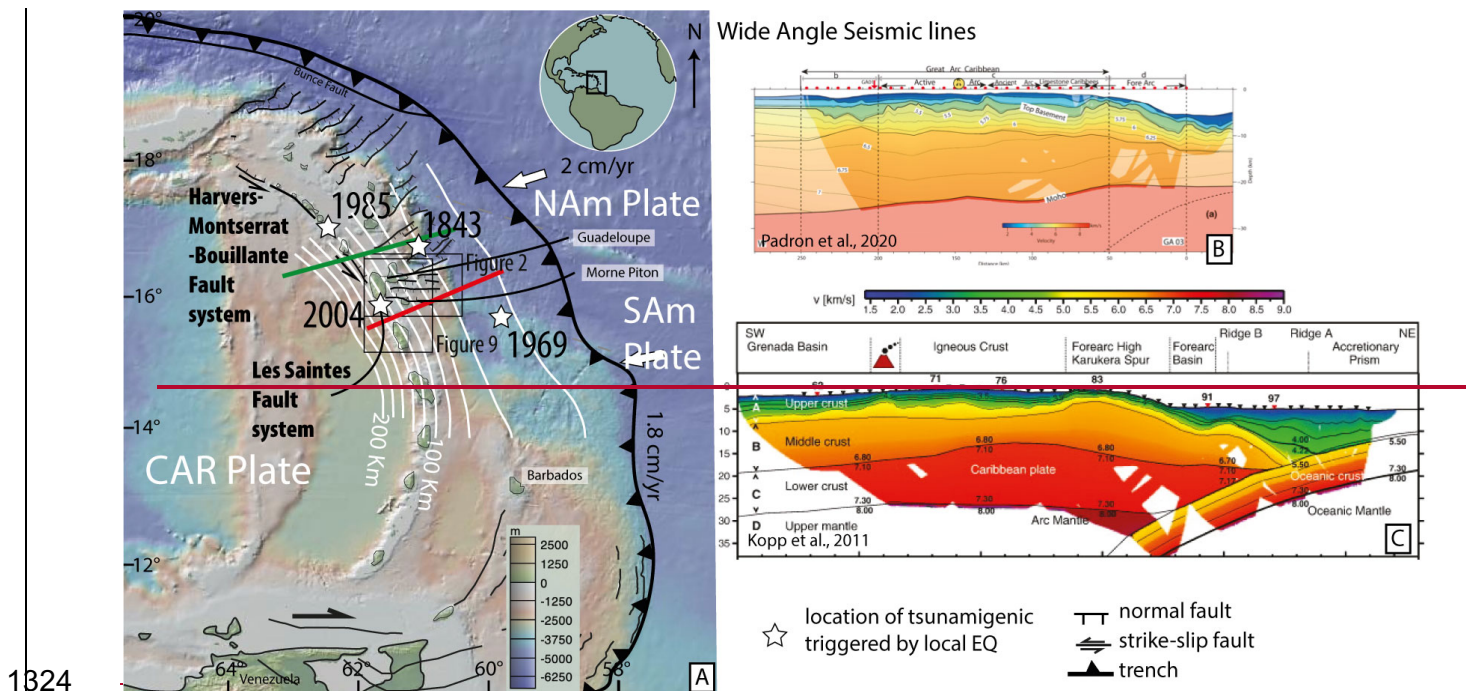
1285 TL/ICMMG (2023). Global Historical Tsunami Database. Institute of Computational Mathematics  
1286 and Mathematical Geophysics SB RAS Tsunami Laboratory, Novosibirsk, Russia,  
1287 <http://tsun.sccc.ru/gtdb/default.aspx> (last accessed on 1 February 2023).

1288 Tronin, A. A., 2009. Satellite remote sensing in seismology. A review. *Remote Sensing*, 2(1), 124-  
1289 150. <https://doi.org/10.3390/rs2010124>

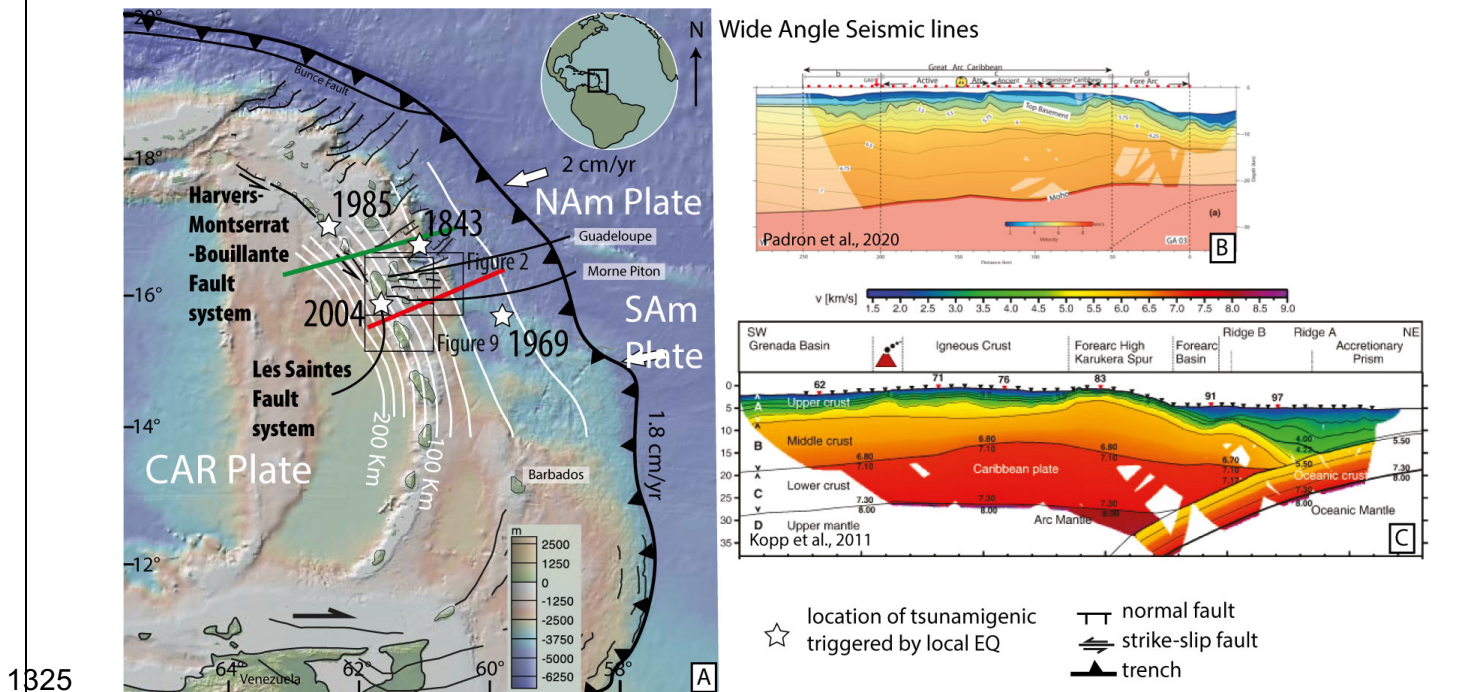


- 1290 van Rijsingen, E. M., Calais, E., Jolivet, R., de Chabalier, J. B., Jara, J., Symithe, S., ... & Ryan, G. A.,  
1291 2021. Inferring interseismic coupling along the lesser antilles arc: A Bayesian approach.  
1292 Journal of Geophysical Research: Solid Earth, 126(2), e2020JB020677.  
1293 <https://doi.org/10.1029/2020JB020677>
- 1294 Wallace, T. C., Helmberger, D. V., & Ebel, J. E., 1981. A broadband study of the 13 August 1978  
1295 Santa Barbara earthquake. *Bulletin of the Seismological Society of America*, 71(6), 1701-  
1296 1718. <https://doi.org/10.1785/BSSA0710061701>
- 1297 Wang, X., 2008. Numerical modelling of surface and internal waves over shallow and  
1298 intermediate water [PhD thesis]. Ithaca (NY): Cornell University. 245 p.
- 1299 Wang, X., Power, W.L., 2011. COMCOT: a tsunami generation, propagation and run-up model.  
1300 Lower Hutt (NZ): GNS Science. 121 p. (GNS Science report; 2011/43).
- 1301 Wang X, Lukovic B, Power WL, Mueller C., 2017. High-resolution inundation modelling with  
1302 explicit buildings. Lower Hutt (NZ): GNS Science. 27 p. (GNS Science report 2017/13).  
1303 <https://doi.org/10.21420/G2RW2N>.
- 1304 Wells, D. L., & Coppersmith, K. J., 1994. New empirical relationships among magnitude, rupture  
1305 length, rupture width, rupture area, and surface displacement. *Bulletin of the seismological*  
1306 *Society of America*, 84(4), 974-1002. <https://doi.org/10.1785/BSSA0840040974>
- 1307 Wessel, P., Luis, J.F., Uieda, L., Scharroo, R., Wobbe, F., Smith, W.H.F., Tian, D., 2019. The Generic  
1308 Mapping Tools Version 6. *Geochemistry, Geophysics, Geosystems*, 20(11), 5556-5564,  
1309 <https://doi.org/10.1029/2019GC008515>.
- 1310 Yamazaki, Y., Cheung, K. F., & Lay, T., 2013. Modeling of the 2011 Tohoku near-field tsunami from  
1311 finite-fault inversion of seismic waves. *Bulletin of the Seismological Society of America*,  
1312 103(2B), 1444-1455. <https://doi.org/10.1785/0120120103>
- 1313 Zahibo, N., Pelinovsky, E., Kurkin, A., & Kozelkov, A., 2003. Estimation of far-field tsunami  
1314 potential for the Caribbean Coast based on numerical simulation. *Science of Tsunami*  
1315 *Hazards*, 21(4), 202-222.
- 1316 Zahibo, N., Pelinovsky, E., Okal, E., Yalçiner, A., Kharif, C., Talipova, T., & Kozelkov, A., 2005. The  
1317 earthquake and tsunami of November 21, 2004 at Les Saintes, Guadeloupe, Lesser Antilles.  
1318 *Science of Tsunami Hazards*, 23(1), 25-39.
- 1319 Zhang, L., Baba, K., Liang, P., Shimizu, H., & Utada, H., 2014. The 2011 Tohoku Tsunami observed  
1320 by an array of ocean bottom electromagnetometers. *Geophysical Research Letters*, 41(14),  
1321 4937-4944. <https://doi.org/10.1002/2014GL060850>

1322

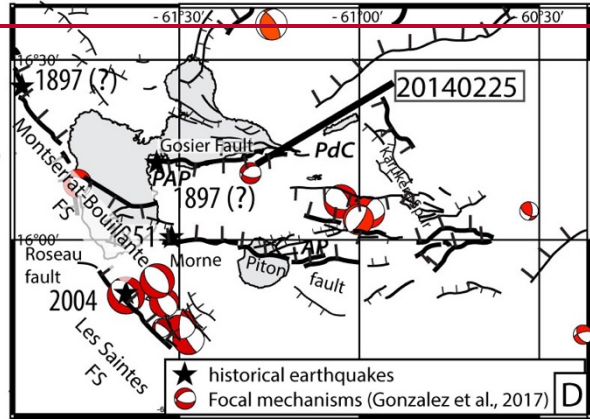
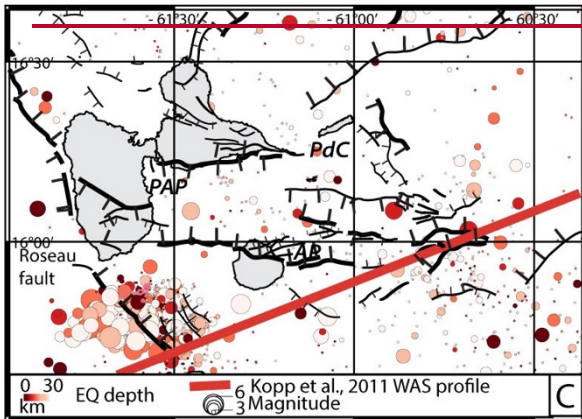
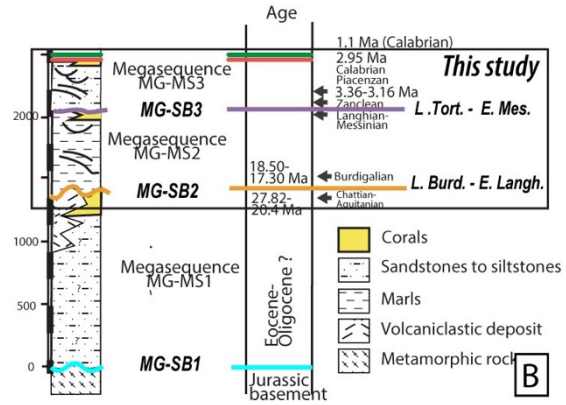
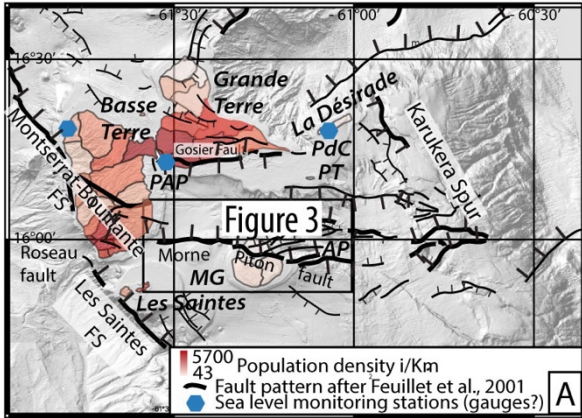


1324

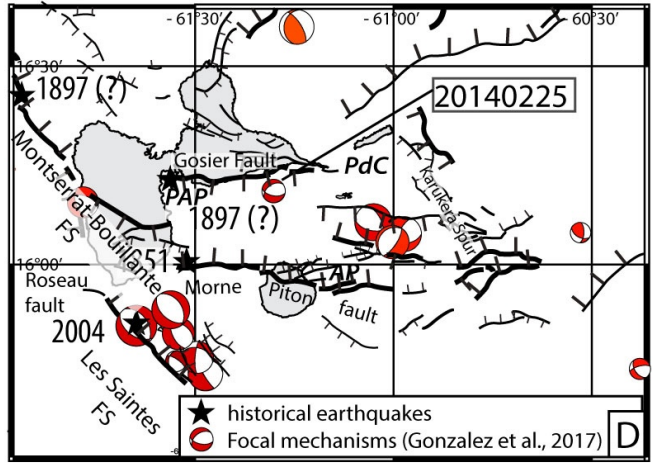
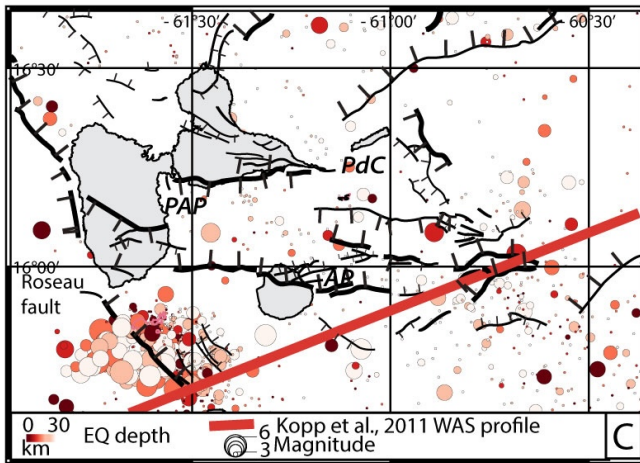
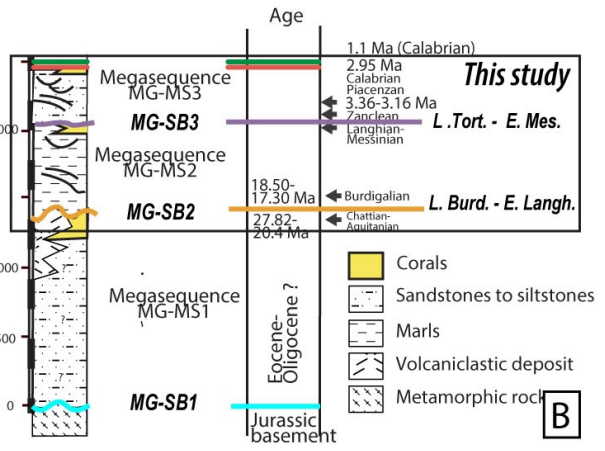
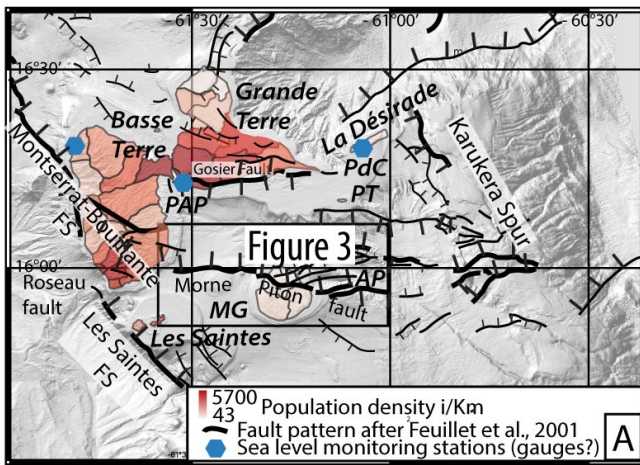


1325

1326 *Figure 1: A: Synthetic tectonic map of the Lesser Antilles forearc. Structures after Feuillet et al.*  
 1327 *(2002), De Min (2014), Laurencin et al. (2019), Legendre (2018), Boucard et al. (2021). Red and*  
 1328 *green thick lines indicate location of the Wide Angle Seismic lines from B. Kopp et al. (2011) and C.*  
 1329 *Padron et al. (2021) respectively. White Star: location of tsunamigenic earthquakes. Thick white*  
 1330 *contour lines: Slab depth isocontour from Bie et al. (2020).*  
 1331

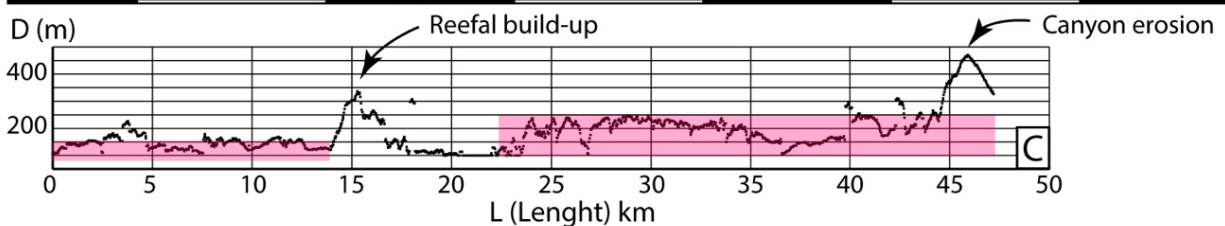
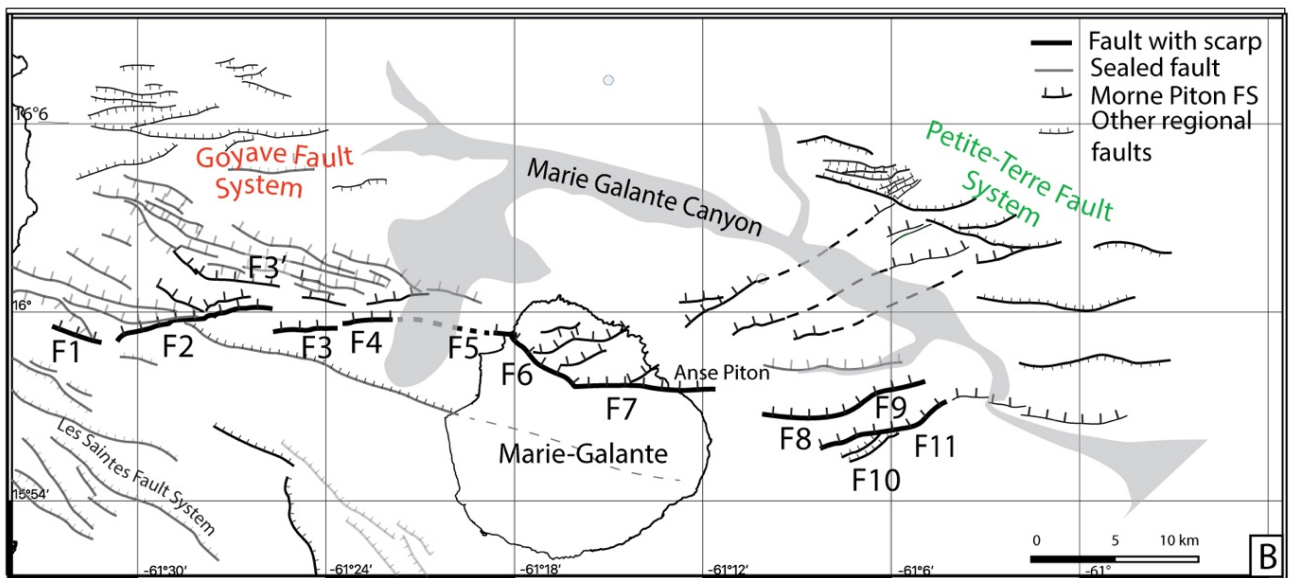
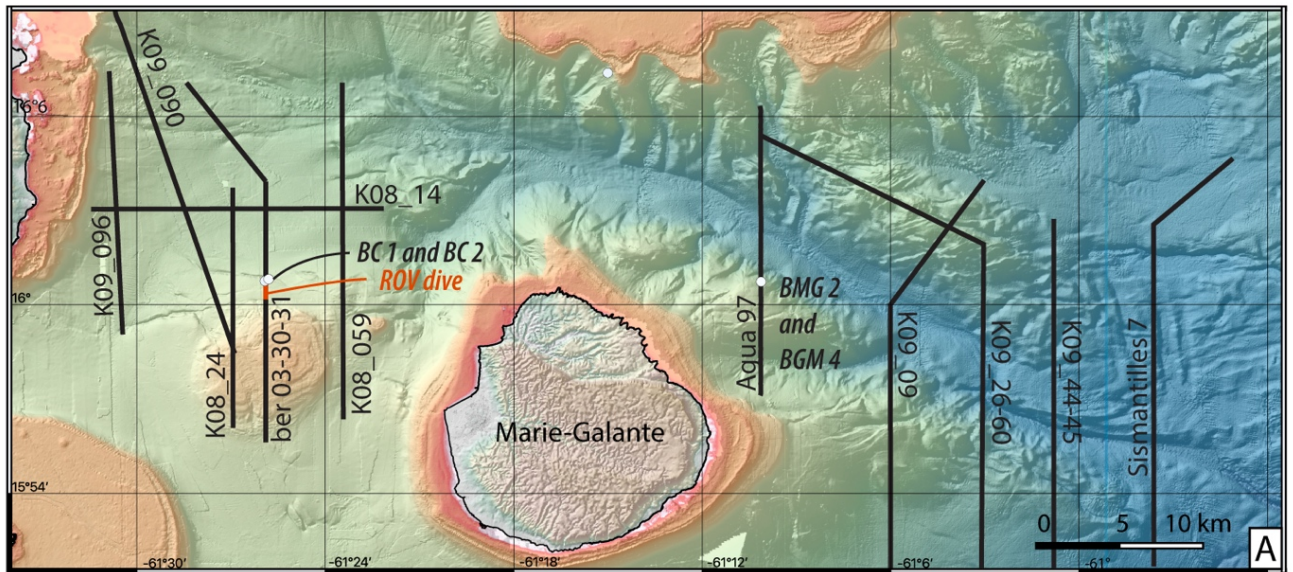


1332

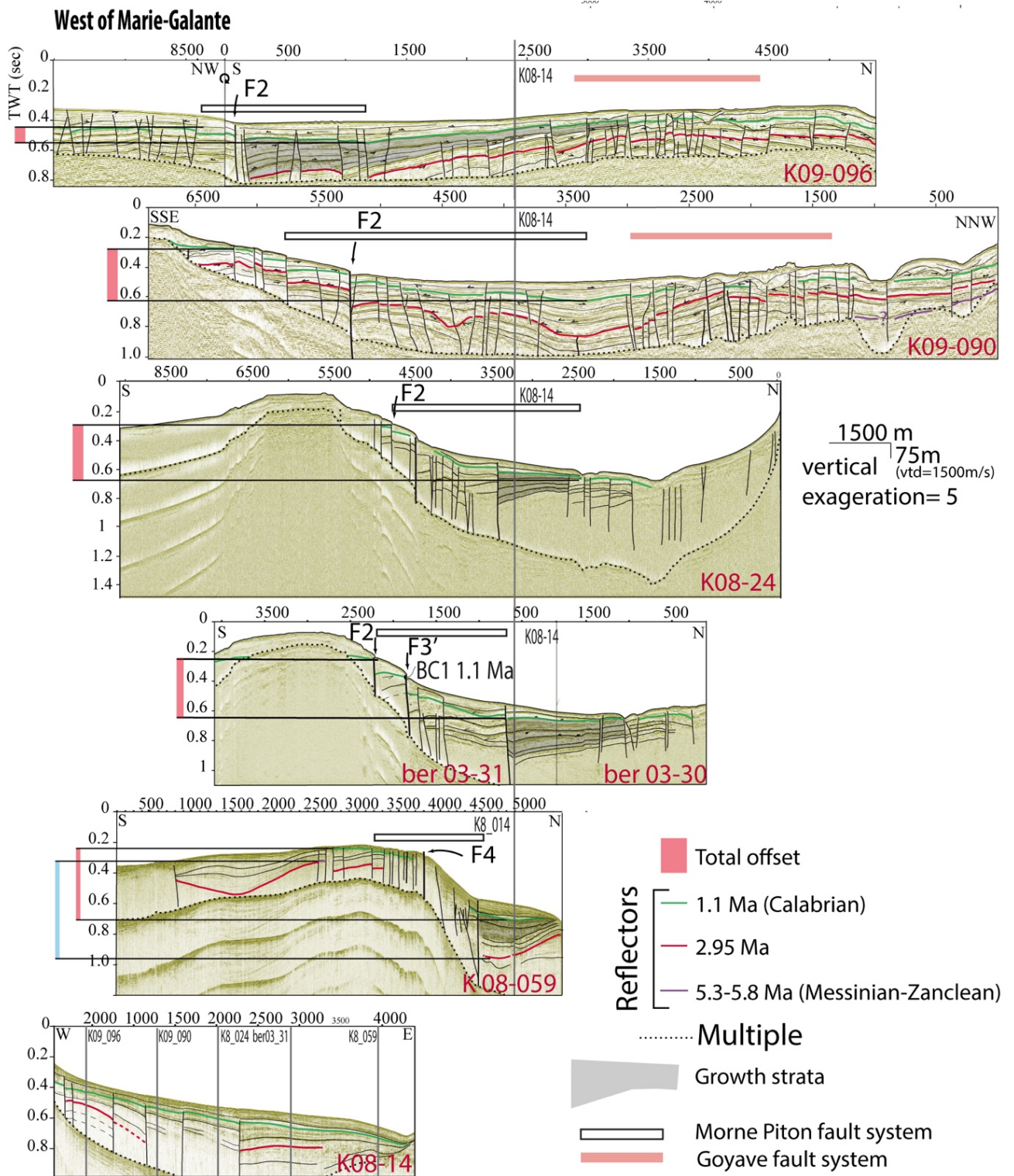


1333

1334 *Figure 2. The Marie-Galante Basin A) structural pattern after Feuillet et al. (2002) and De Min et*  
1335 *al. (2015) on the shaded-relief bathymetric map. blue hexagons : tide gauges*  
1336 *<http://refmar.shom.fr/fr/liste-maregraphes-data.shom.fr>. Red colors scale: Guadeloupe*  
1337 *population density per km2 after GEOFLA (<https://www.data.gouv.fr/fr/datasets/geofla-r/>). B)*  
1338 *Sismostratigraphic scheme of the Marie-Galante basin modified after Cornée et al., 2023. C) Colored*  
1339 *dots: Crustal seismicity (from IRIS seismic database 2023) for magnitude earthquakes (EQ)*  
1340  *$3 > M_w > 6.5$  and located from 0 to 30 km depth), red line locates the WAS line (Kopp et al., 2011).*  
1341 *D) Focal mechanisms solutions are indicated by red beachballs after Gonzalez et al. (2017). The*  
1342 *location of historical earthquakes is indicated by black stars (after: Feuillet et al., 2011b). AP, PdC,*  
1343 *PAP, PT stand for Anse Piton, Pointe des Chateaux, Pointe-à-Pitre and Petite Terre.*  
1344



1345  
 1346 Figure 3. A) High resolution (25m grid spacing) bathymetric map [UMO16] of the Marie-Galante Basin,  
 1347 offshore Guadeloupe and location of the seismic profiles shown on figures 4 and 5, and location of  
 1348 dredge samples used for the seismic units age calibration (Münch et al. 2013). B) Structural  
 1349 interpretation of the E-W trending Morne Piton Fault system. C) A proxy for cumulative strain given  
 1350 by the graphic displaying the D (fault surface displacement) taken as the difference between the top  
 1351 and the toe of the fault scarp versus L (fault length) along the whole system.

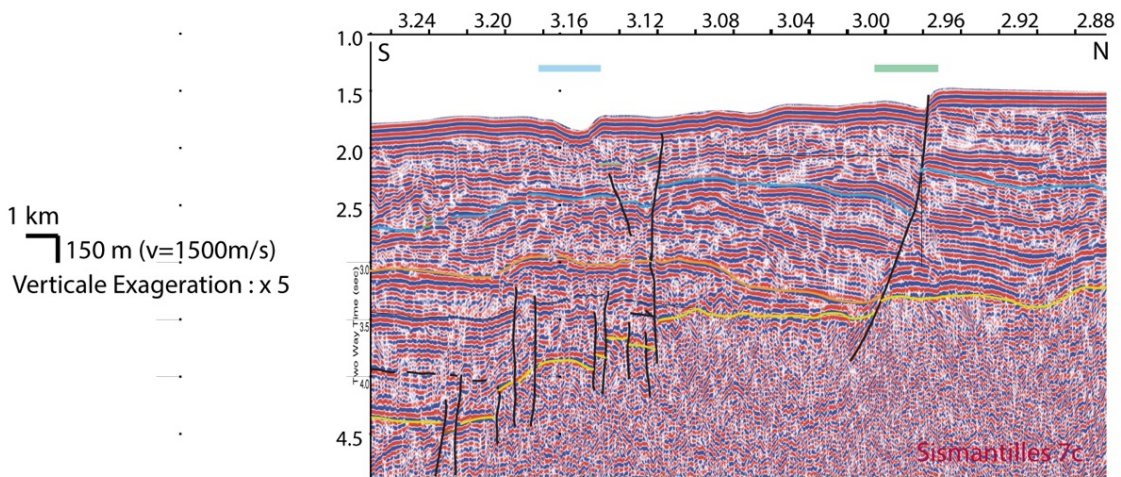
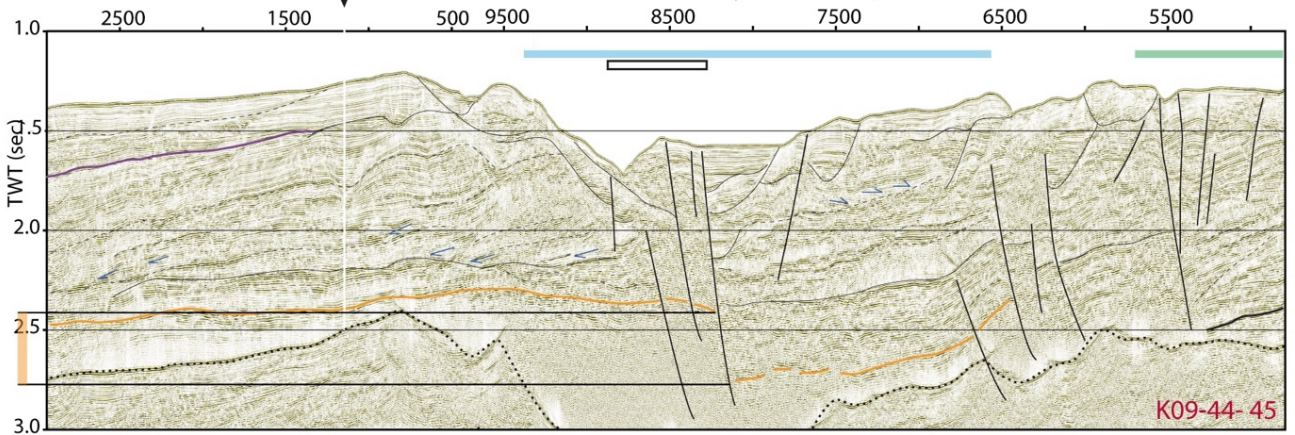
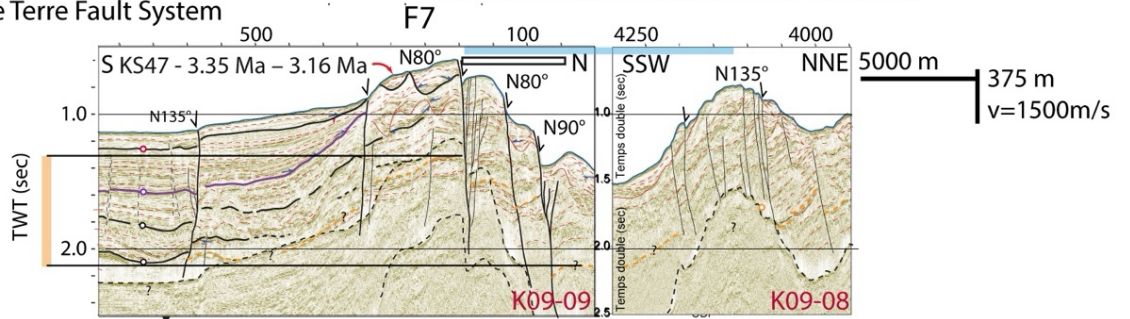
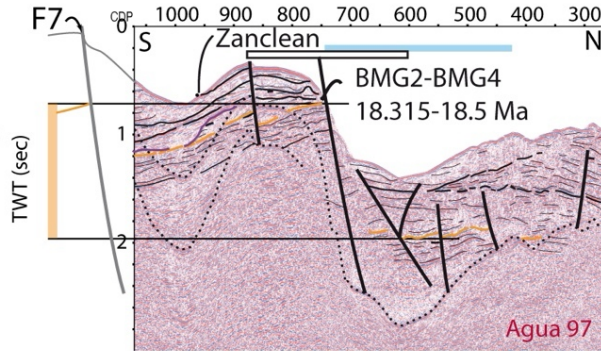


1352  
 1353 *Figure 4: Seismic lines West of Marie-Galante (location on Figure 3) showing the correlation across*  
 1354 *the Morne Piton fault system of the 1.29Ma unit reflector (Green) that correspond to the reflector*  
 1355 *dredged at BC1 and BC2 location along the Ber03\_30-31 seismic line. The 2.95Ma Unit Boundary*  
 1356 *(Red) is correlated from seismic lines south of the Colombie Bank and Eastern Marie-Galante Basin*  
 1357 *(line K09\_90 and K09\_26-62 location on figure 2). Notice that the basin sedimentary slope is in the*

1358 E-W direction (parallel to line K08-14). Therefore, the initial topography of the reflectors in the N-  
 1359 S direction, across the fault system, can be neglected when measuring the offset along the seismic  
 1360 lines.

**East of Marie-Galante**

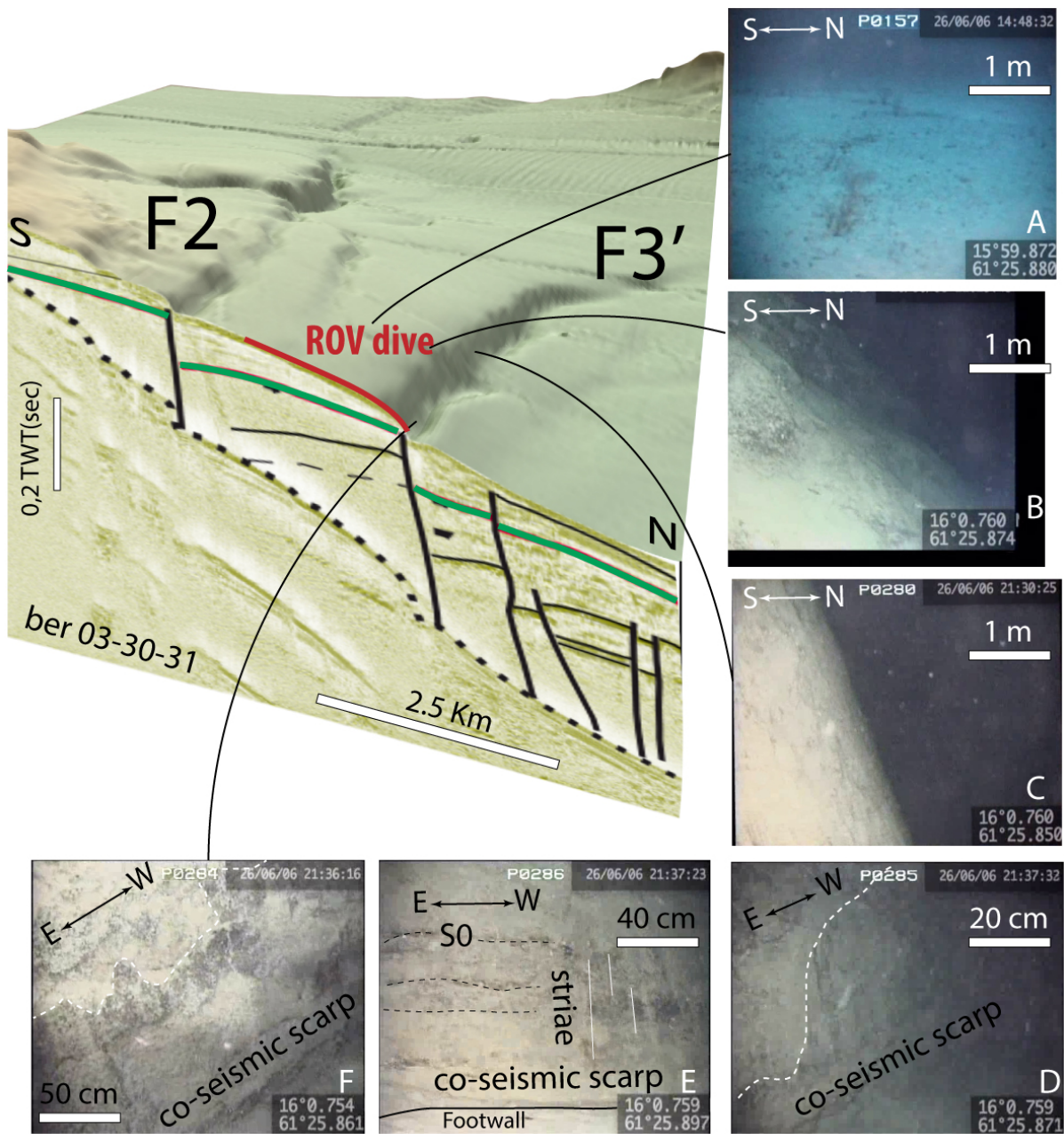
- █ Total offset
- Reflectors
  - 5.3-5.8 Ma (Messinian-Zanclean)
  - 18.3-18.5 Ma (Upper Burigalian)
  - igneous basement
  - ..... Multiple
- Marie-Galante Canyon
- Morne Piton fault system
- Petite Terre Fault System



1361

1362 Figure 5: Seismic lines east of Marie-Galante illustrate the correlation across the Morne Piton fault system of the 7 Ma (Tortonian/Messinian) MG-SB3 sequence boundary (Purple) and the 16 Ma, (Burdigalian) MG-SB2 Sequence Boundary (Orange). Seismic line location on Figure 3).

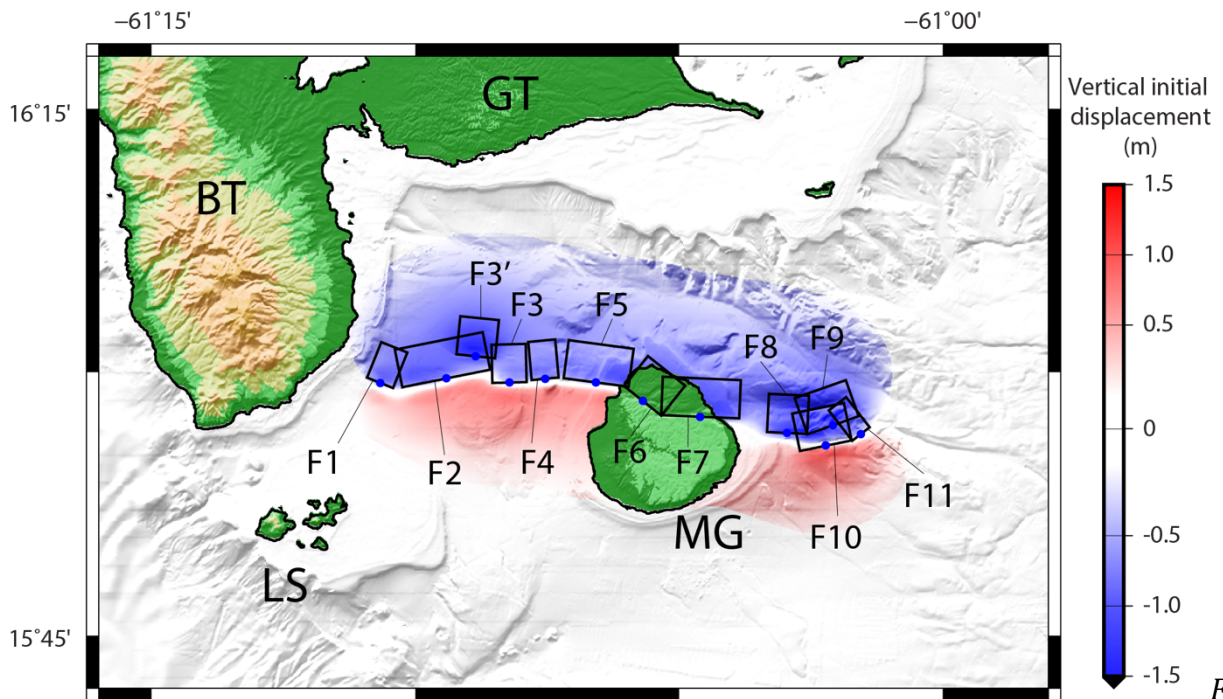
1365



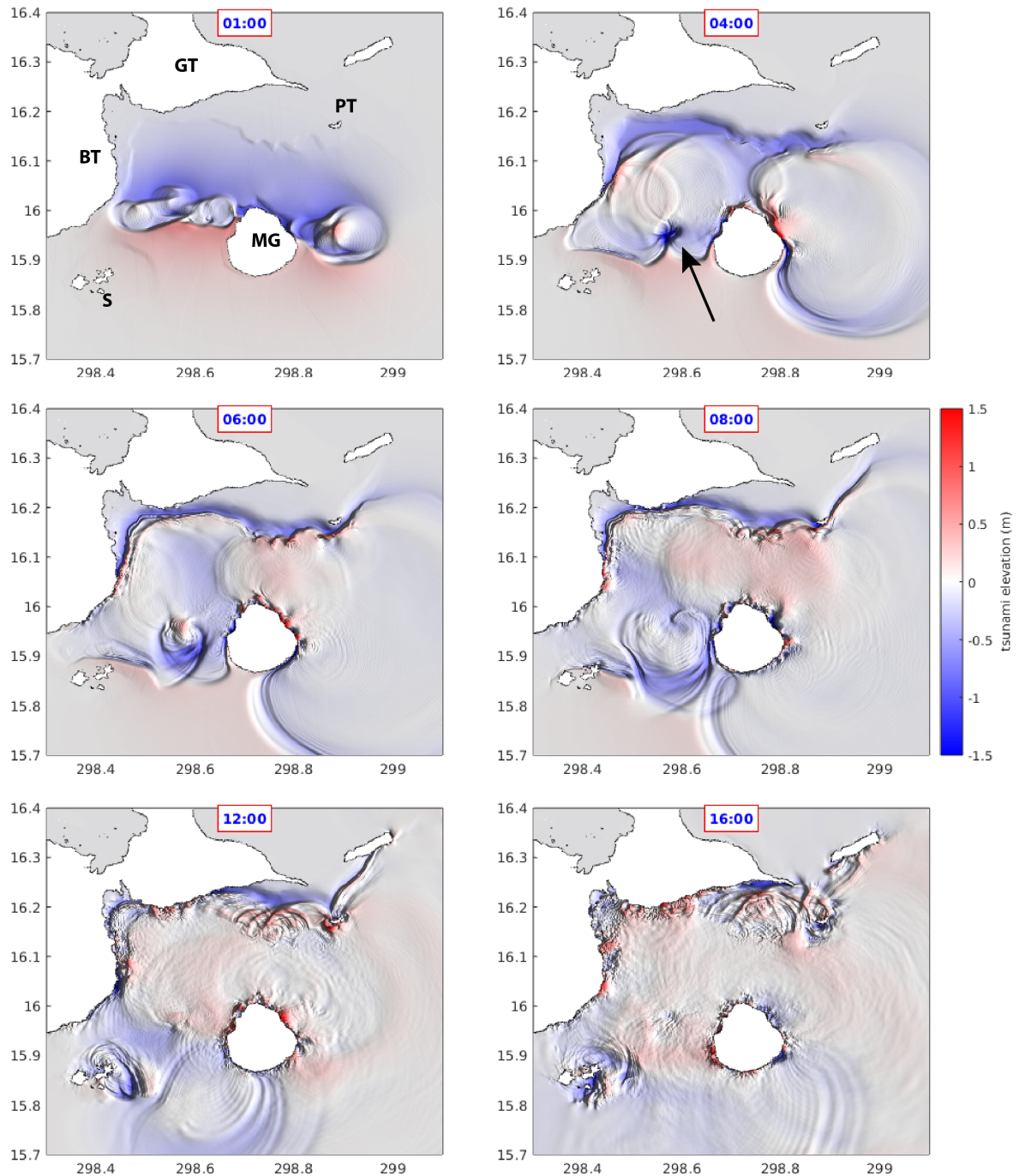
1366 Figure 6: ROV photographs of fault identified on the seafloor along the BER03-30-31 seismic line across the F3' Morne Piton fault segment (location on Figure 3). (A) photograph of the hangingwall of F3'. The eroded F3' fault plane presents a progressive downward slope steepening (B and C) until the toe of the fault, which is marked by a characteristic co-seismic scarp with a dip slip striae (D E F). On each photograph, white numbers starting with a P is the water depth in meters Latitude is North and Longitude is West (WGS84). A B and C views show several tens square meters wide areas,



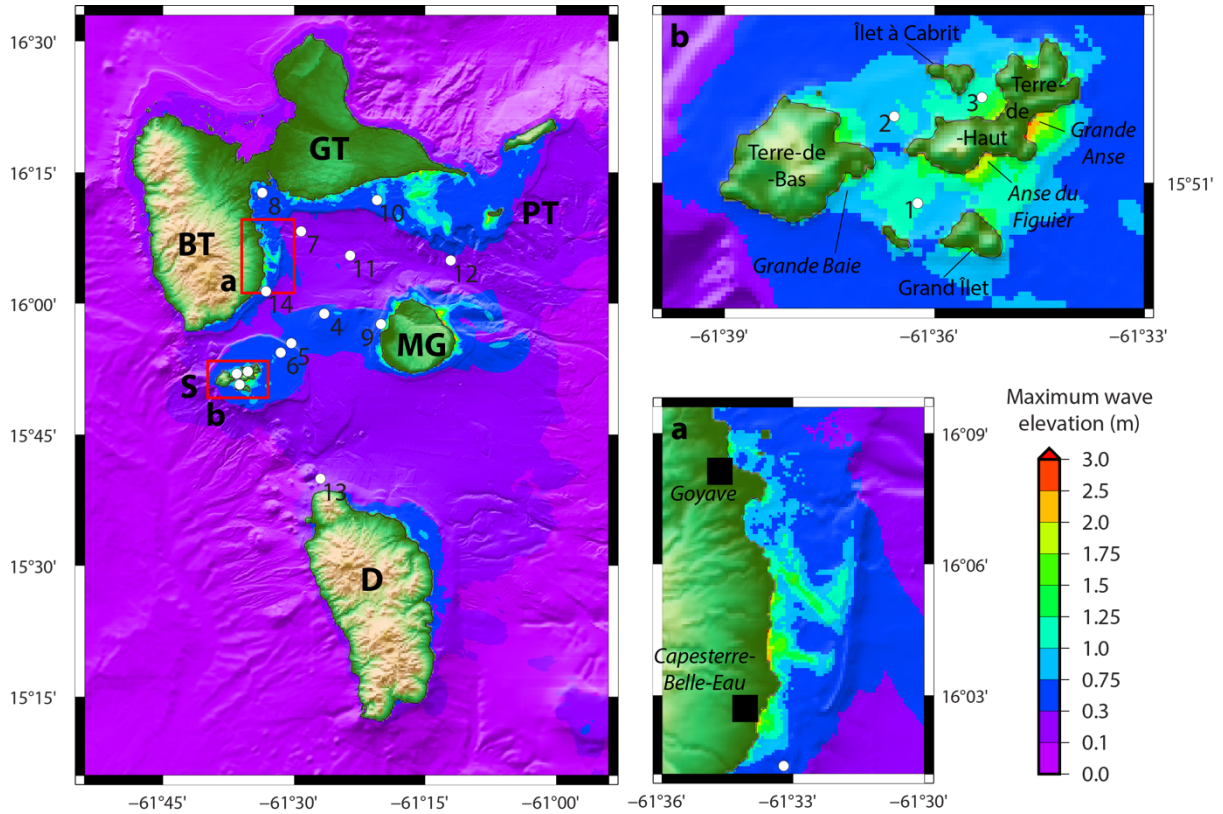
1373 D E F are close up showing ca 1m high escarpment just above the foot of the fault scarp (visible at  
1374 the bottom of each photos).  
1375



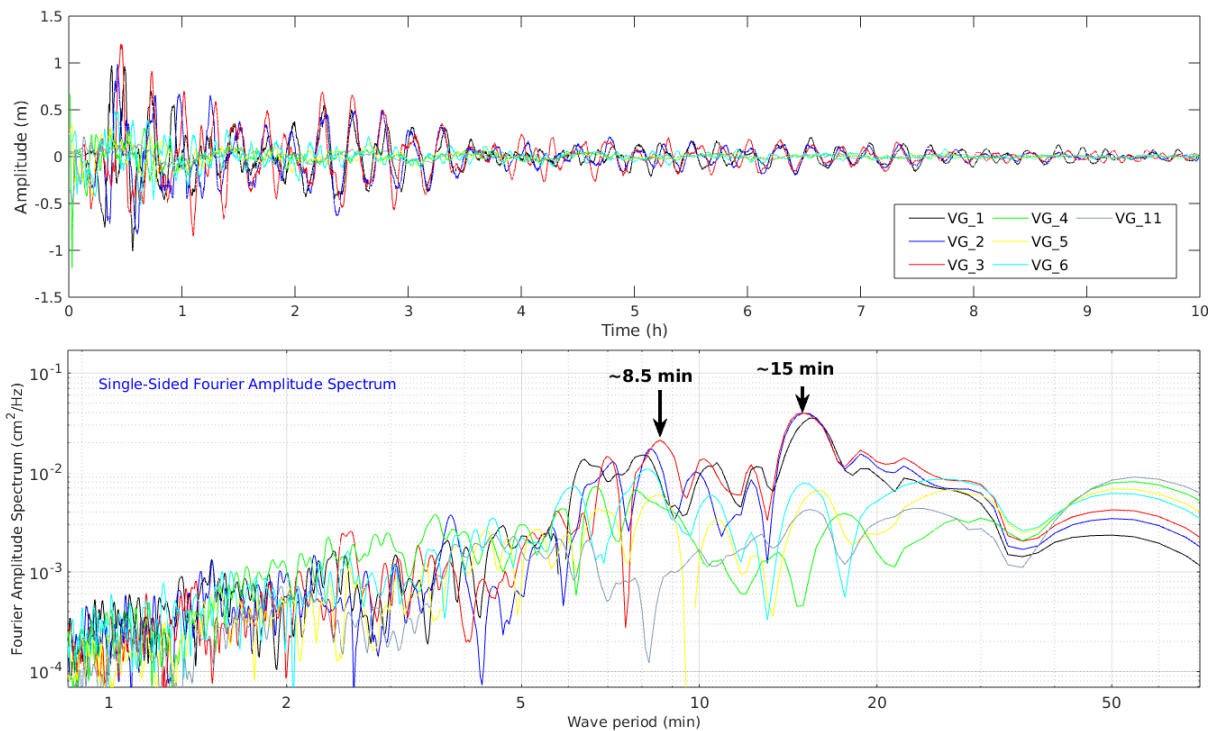
1376  
1377 *Figure 7: Initial surface elevation for a maximum credible scenario built with the 11 fault segments*  
1378 *detailed in Table 3. Blue dots indicate the top fault center. Acronyms stand for Grande-Terre (GT),*  
1379 *Basse-Terre (BT), Les Saintes (LS) and Marie-Galante (MG).*



1380  
 1381 *Figure 8: Snapshots of tsunami elevation within the Guadeloupe Archipelago at 1, 4, 8, 6, 12 and 16*  
 1382 *minutes of waves propagation. Red and blue colors correspond to wave crests and troughs*  
 1383 *respectively. The black arrow shows the Banc Colombie shoal. BT: Basse-Terre; GT: Grande-Terre;*  
 1384 *S: Les Saintes; PT : Petite-Terre ; MG : Marie-Galante.*

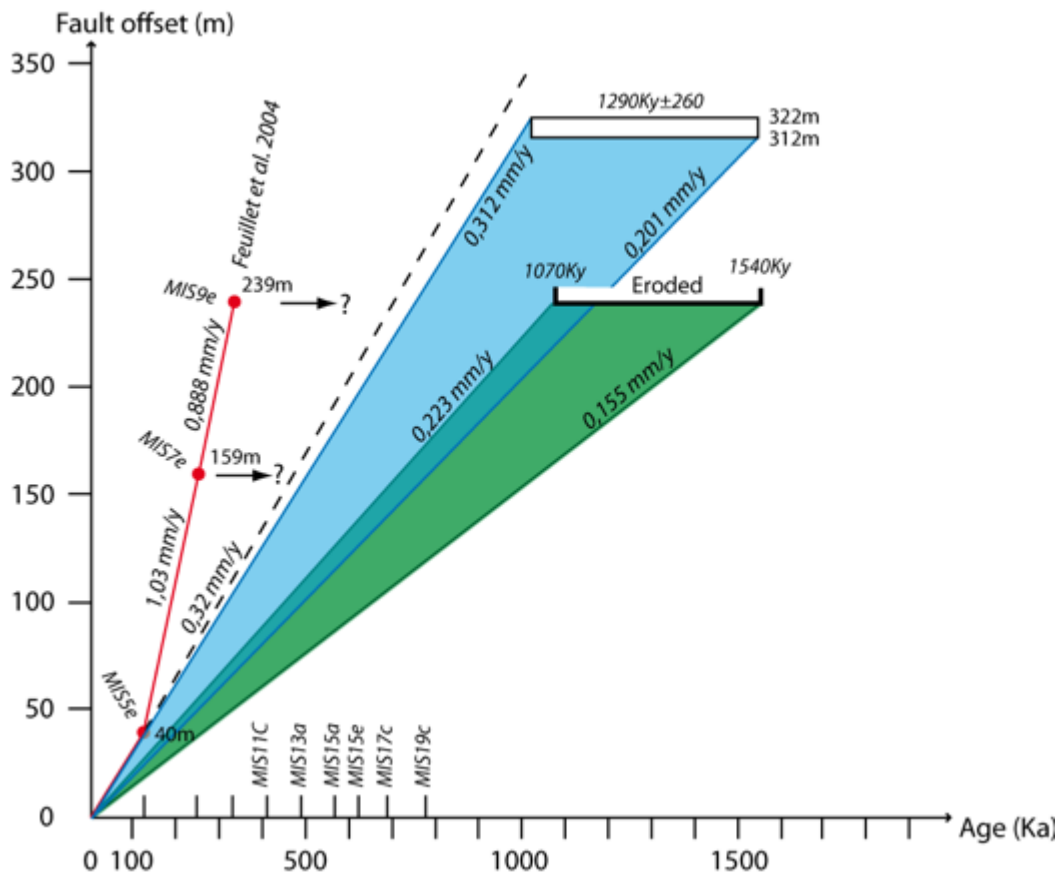


1385  
 1386 *Figure 9: Shadowed bathymetric map with tsunami maximum wave elevation. Numbered white*  
 1387 *dots: fourteen virtual sea-level gauges (VG) : . BT: Basse-Terre; GT: Grande-Terre; S: Les Saintes; PT*  
 1388 *: Petite-Terre ; MG : Marie-Galante ; D : Dominica. VG\_4 & VG\_11 are located near the fault rupture*  
 1389 *region, the VG\_5 & VG\_6 are near the Les Saintes Fault system. VG\_1, VG\_2 & VG\_3 are within the*  
 1390 *Les Saintes archipelago.*



1391

1392 Figure 10: Post-processing of virtual gauge records. Top: sea-level records at 7 different locations  
 1393 (VG 1 to 6 and VG11 – location on figure 9); bottom: single-sided Fourier amplitude spectrum. The  
 1394 blue arrows symbolize the location of the 2 peaks of period ~6.5 and 17 min.



1395  
 1396 Figure 11: Fault offset along the Morne Piton Fault against the age of the strain marker. Red: data  
 1397 from Feuillet et al. (2004) based on absolute age of terrace T4 (MIS5e), the estimated age of terrace  
 1398 T2 (MIS7e) and the suggested age of Marie-Galante upper plateau (MIS9e). Green: strain range  
 1399 calculated using upper plateau unit age from Münch et al. (2014) (note that erosion may lower this  
 1400 estimation strain rate). Blue: strain range calculated from the fault offset of the seismic unit dated  
 1401 ca 1,2Ma along the seismic line K08-59 (green reflector on Figure 4). Dotted line indicates the 0.32  
 1402  $\text{mm}\cdot\text{yr}^{-1}$  strain rate from the estimated offset of the MIS5e Terrace in Marie-Galante  
 1403 (Feuillet et al. 2004).

1404

Cruise	KaShallow 1	KaShallow 2	Aguadomar	SismAntilles	GEOBERYX03 SISM BGM
Seismic source	1000 J sparker	35-45 in3 GI Airguns array	45-105 in3 Two GI Airguns	4400 in3 Airguns array.	1000 J sparker
Peak frequency (far field)	250-400Hz	40-70Hz	30-50Hz	15-20Hz	250-400Hz
Number of traces	6 traces	72 traces	6 traces	360 traces	6 traces
Fold coverage	3/6 fold	9/18 fold	3 fold	30 fold	3/6 fold
Inter CDP distance	4 m	3.125 m	4 m	6,25 m	4 m

1405  
1406 *Table 1: Main acquisition parameters of the seismic data shown in this study (Figures 4 and 5).*

1407

Profile Name Ported from East to West	Age (Ma)	Uncer tainty (Ma)	horizon depth in the footwall (stwt)		horizon depth in the hangingwall (stwt)		Ven m/s 2500		Ven m/s 2500		Ven m/s 2000		Ven m/s 2000		TOTAL OFFSET (m)		TOTAL OFFSET (m)		Strain rate (mm/years)			Interval strain rate (mm/yrs )
			water	rock	water	rock	max	min	max	min	max	min	max	min	max	min	max	Average	nty			
																				min	max	
K09-44-45 – MG-SB2	16	1	1,575	0,83	1,575	1,2	2 212,5	2 700,0	2 006,3	2 396,3	487,5	390,0	0,046	0,089	0,067	0,030						
since inception	7	1,5																				
K09_08-09 – MG-SB2	16	1	0,595	0,91	1,27	0,9	1 577,5	2 052,5	1 351,3	1 832,5	475,0	481,3										
since inception	7	1,5																				
Agua 97 – MG-SB2	16	1	0,05	0,72	1,36	0,6	937,5	1 770,0	757,5	1 620,0	832,5	862,5										
since inception	7	1,5																				
<b>UB4</b>	<b>2,95</b>	<b>0,05</b>	<b>0,23</b>	<b>0,09</b>	<b>0,59</b>	<b>0,4</b>	<b>285,0</b>	<b>905,0</b>	<b>262,5</b>	<b>812,5</b>	<b>620,0</b>	<b>550,0</b>	<b>0,183</b>	<b>0,214</b>	<b>0,199</b>	<b>0,022</b>	<b>0,16</b>					
K08-059	1,29	0,26	0,22	0,02	0,5	0,1	190,0	512,5	185,0	485,0	322,5	300,0	0,194	0,313	0,253	0,085	0,25					
Ber 03-31	1,29	0,26	0,21	0,04	0,53	0,1	207,5	522,5	197,5	497,5	315,0	300,0	0,194	0,306	0,250	0,079						
K08-24	1,29	0,26	0,25	0,04	0,6	0	237,5	487,5	227,5	480,0	250,0	252,5	0,163	0,243	0,203	0,056						
K09-090	1,29	0,26	0,33	0,02	0,49	0,1	272,5	530,0	267,5	497,5	257,5	230,0	0,148	0,250	0,199	0,072						
K09-096	1,29	0,26	0,32	0,12	0,44	0,1	390,0	505,0	360,0	470,0	115,0	110,0	0,071	0,112	0,091	0,029						

1409 Table 2: Measured offset of seismic reflectors across the Morne Piton fault system and calculated  
1410 total vertical strain rates. See text for the ages estimate. Seismic reflectors depth on each side of the  
1411 fault system is measured in time (stwt – second two way time) and converted in depth in using water  
1412 velocity (1500m/s) and two end-member velocities for the sediment (see text for explanation),  
1413 providing a minimum and a maximum offset value. The minimum strain rate is obtained from the  
1414 ratio between the min offset and the max age bound of the reflector and vice versa.  
1415

Fault segment	Lon (°)	Lat (°)	Length (m)	Width (m)	Top of the fault plane depth (m)	Strike (°)	Dip (°)	Rake (°)	Slip (m)
F1	-61.5335	15.98987	2838	12500	500	111	75	-90	1.89
F2	-61.4708	15.994	9070	12500	500	78	75	-90	1.89
F3'	-61.4428	16.01503	3918	12500	500	95	75	-90	1.89
F3	-61.4108	15.99009	3474	12500	500	88	75	-90	1.89
F4	-61.377	15.99367	2735	12500	500	84	75	-90	1.89
F5	-61.3287	15.99021	6623	12500	500	97	75	-90	1.89
F6	-61.2846	15.97275	4813	12500	500	128	75	-90	1.89
F7	-61.2301	15.95767	7904	12500	500	92	75	-90	1.89
F8	-61.1477	15.94221	4052	12500	500	92	75	-90	1.89
F9	-61.1042	15.94958	5495	12500	500	70	75	-90	1.89
F10	-61.111	15.93014	5336	12500	500	78	75	-90	1.89
F11	-61.0777	15.94126	2228	12500	500	52	75	-90	1.89

1416  
1417 Table 3: Parameters used for the tsunami source simulation of a rupture along the multisegment  
1418 fault presented in figure 7.  
1419